Research Square

Preprints are preliminary reports that have not undergone peer review.
They should not be considered conclusive, used to inform clinical practice,
or referenced by the media as validated information.

War-Related Factors and Conditional Scenario Estimates of Registered Cancer Deaths in Gaza: A Systematic Review, Meta-Analysis, and Monte Carlo Simulation Study

guangneng zhu
North Sichuan Medical College
Wei Zhang
North Sichuan Medical College, Nanchong, Sichuan, China
Shen Li
Sichuan University, Chengdu, Sichuan, China
Hani Salman Ayyash
Turkish Palestinian Friendship Hospital, Gaza, Palestine
Belal Aldabbour
Islamic University of Gaza, Gaza, Palestine
Amal Al Omari
King Hussein Cancer Center, Amman, Jordan
Bayan Ahmad
King Hussein Cancer Center, Amman, Jordan
Shipeng Hu
Peking University, Beijing, China
Xinyu Xu
North Sichuan Medical College, Nanchong, Sichuan, China
Hexian Zhang
University of Hong Kong, Hong Kong, China
Jiahui Guan
University of Hong Kong, Hong Kong, China
Haowei Ma
Case Western Reserve University, Cleveland, USA
Hongying Li
North Sichuan Medical College, Nanchong, Sichuan, China
Diaa Isayed
Istishari Arab Hospital, Ramallah, Palestine
Ammar Nawfal
Istishari Arab Hospital, Ramallah, Palestine

Noor Jawabreh
Istishari Arab Hospital, Ramallah, Palestine
Saher Tayeh
Istishari Arab Hospital, Ramallah, Palestine
Salah Safi
Salah Safi Dermatology and Laser Clinic, Ramallah, Palestine
Imad Shalalde
Palestine Red Crescent Hospital, Ramallah, Palestine
Ruqaya Faqeeh
German Palestinian Medical Centre, Ramallah, Palestine
Abdullah Zahran
Palestine Medical Complex, Ramallah, Palestine
Tammam Zyoud
Palestine Medical Complex, Ramallah, Palestine
Ihab Anbar
Ram Dental Clinic, Ramallah, Palestine
Fadi Ayyash
Karmel Medical Centre, Biddu, Jerusalem, Palestine
Fahim Abu Soboh
Palestine Medical Complex, Ramallah, Palestine
Abdallah Yousef
Palestine Medical Complex, Ramallah, Palestine
Saadah Jaber
Dr. Jaber Gynaecology-Oncology Clinic, Ramallah, Palestine
Asem Mansour
Amansour@khcc.jo

King Hussein Cancer Center, Amman, Jordan
Youwen Yang
yangyouwen@jxust.edu.cn

Jiangxi University of Science and Technology, Ganzhou 341000, China
Mohamed Abu Nada
mabunada333@yahoo.com

Turkish Palestinian Friendship Hospital, Gaza, Palestine
Ali Albelbesi
alialbelbeisi@gmail.com

Palestinian Ministry of Health, Gaza, Palestine
Aymen Elsous
aymanalsoos65@gmail.com

Palestinian Ministry of Health, Gaza, Palestine
Yuelong Ji
jiyuelong@ai-research.group

Peking University, Beijing, China
Huda Lahham
huda.lahham@gmail.com

Palestinian Ministry of Health, Ramallah, Palestine
Ola Al-Najjar
ol_najjar@yahoo.com

Palestinian Ministry of Health, Gaza, Palestine
Yueshan Pang
469627639@qq.com

North Sichuan Medical College, Nanchong, Sichuan, China
Salwa Massad
massads@who.int

World Health Organization, Jerusalem, Palestine
Shahmir H. Ali
sali@nus.edu.sg

National University of Singapore, Singapore
Sukun Tian
sukhum169@hotmail.com

Peking University, Beijing, China
Zining Luo
rosin@ai-research.group

North Sichuan Medical College, Nanchong, Sichuan, China; University of Hong Kong, Hong Kong, China

Junwen Wang

junwen@hku.hk

University of Hong Kong, Hong Kong, China

Jiebin Xie

xiejiebin84@126.com

North Sichuan Medical College, Nanchong, Sichuan, China

Shaymaa AlWaheidi

shaymaa.al-waheidi@kcl.ac.uk

International Agency for Research on Cancer (IARC), Lyon, France

Hussein ALMasri

halmasri81@staff.alquds.edu

Al-Quds University, Jerusalem, Palestine

Research Article

Keywords:

Posted Date: November 6th, 2026

DOI: https://doi.org/10.21203/rs.3.rs-11625485/v1

License: This work is licensed under a Creative Commons Attribution 4.0 International License.
Read Full License

Additional Declarations: The authors declare no competing interests.

War-Related Factors and Conditional Scenario Estimates of Registered Cancer Deaths in Gaza: A Systematic Review, Meta-Analysis, and Monte Carlo Simulation Study

Authors

Guangneng Zhu[1¶], Wei Zhang[1¶], Shen Li[2¶], Hani Salman Ayyash[3¶], Belal Aldabbour[4¶], Amal Al Omari[5¶], Bayan Ahmad[5¶], Shipeng Hu[6¶], Xinyu Xu[1¶], Hexian Zhang[7], Jiahui Guan[7], Haowei Ma[8], Hongying Li[1], Diaa Isayed[9], Ammar Nawfal[9], Noor Jawabreh[9], Saher Tayeh[9], Salah Safi[10], Imad Shalalde[11], Ruqaya Faqeeh[12], Abdullah Zahran[13], Tammam Zyoud[13], Ihab Anbar[14], Fadi Ayyash[15], Fahim Abu Soboh[13], Abdallah Yousef[13], Saadah Jaber[16], Asem Mansour[5†], Youwen Yang[17†], Mohamed Abu Nada[3†], Ali Albelbesi[18†], Aymen Elsous[18†], Yuelong Ji[6†], Huda Lahham[19†], Ola Al-Najjar[18†], Yueshan Pang[1†], Salwa Massad[20†], Shahmir H. Ali[21†], Sukun Tian[6†], Zining Luo[1†], Junwen Wang[7†], Jiebin Xie[1†], Shaymaa AlWaheidi[22†], Hussein ALMasri[23†]

Affiliations

1. North Sichuan Medical College, Nanchong, Sichuan, China
2. Sichuan University, Chengdu, Sichuan, China
3. Turkish Palestinian Friendship Hospital, Gaza, Palestine
4. Islamic University of Gaza, Gaza, Palestine
5. King Hussein Cancer Center, Amman, Jordan
6. Peking University, Beijing, China
7. University of Hong Kong, Hong Kong, China
8. Case Western Reserve University, Cleveland, USA
9. Istishari Arab Hospital, Ramallah, Palestine
10. Salah Safi Dermatology and Laser Clinic, Ramallah, Palestine
11. Palestine Red Crescent Hospital, Ramallah, Palestine
12. German Palestinian Medical Centre, Ramallah, Palestine
13. Palestine Medical Complex, Ramallah, Palestine
14. Ram Dental Clinic, Ramallah, Palestine
15. Karmel Medical Centre, Biddu, Jerusalem, Palestine
16. Dr. Jaber Gynaecology-Oncology Clinic, Ramallah, Palestine
17. Jiangxi University of Science and Technology, Ganzhou 341000, China
18. Palestinian Ministry of Health, Gaza, Palestine
19. Palestinian Ministry of Health, Ramallah, Palestine
20. World Health Organization, Jerusalem, Palestine
21. National University of Singapore, Singapore
22. International Agency for Research on Cancer (IARC), Lyon, France
23. Al-Quds University, Jerusalem, Palestine

¶ These authors contributed equally.

† Corresponding authors.

Corresponding author emails

Asem Mansour: Amansour@khcc.jo; **Youwen Yang:** yangyouwen@jxust.edu.cn; **Mohamed Abu Nada:** mabunada333@yahoo.com; **Ali Albelbesi:** alialbelbeisi@gmail.com; **Aymen Elsous:** aymanalsoos65@gmail.com; **Yuelong Ji:** jiyuelong@ai-research.group; **Huda Lahham:** huda.lahham@gmail.com; **Ola Al-Najjar:** ol_najjar@yahoo.com; **Yueshan Pang:** 469627639@qq.com; **Salwa Massad:** massads@who.int; **Shahmir H. Ali:** sali@nus.edu.sg; **Sukun Tian:** sukhum169@hotmail.com; **Zining Luo:** rosin@ai-research.group; **Junwen Wang:** junwen@hku.hk; **Jiebin Xie:** xiejiebin84@126.com; **Shaymaa AlWaheidi:** shaymaa.al-waheidi@kcl.ac.uk; **Hussein ALMasri:** halmasri81@staff.alquds.edu

Ethics declarations

Competing interests

The authors declare no competing interests.

Data availability

The corresponding author had full access to all data in the study and final responsibility for the decision to submit the report for publication. The data used and analyzed during the current study are available from the corresponding author upon reasonable request.

Code availability

The code used to generate the factor standardization figures and to conduct the meta-analyses, the counterfactual baseline extrapolation of registered cancer deaths, and the primary six-factor joint modeling and six-factor principal analysis plus exploratory extension is available at: https://github.com/zhuguangneng/Drawing-Code.

Abstract

Objective: To identify war-related factors affecting patients with cancer, synthesize their associations with cancer-specific mortality, and estimate changes in registered cancer deaths under multifactor scenarios in Gaza during October–December 2023.

Methods: PubMed, Web of Science, Embase, and Cochrane Library were searched. Two reviewers independently screened studies, extracted factors, and identified a cancer-patient subset. Cancer-specific mortality or survival effects were pooled for six factor groups using REML random-effects models. Gaza registered cancer deaths and population data from 2016–2022 were used to estimate a 2023 counterfactual registry baseline with a Pearson-dispersion-corrected Poisson model and 100,000 Monte Carlo simulations. Five non-environmental factors were combined with treatment delay or interruption in a primary six-factor joint model. Particulate-matter exposure was included only in exploratory analyses.

Results: The review identified 1,341 factor records from 413 studies and 263 standardized factors. The cancer subset contained 23 studies, 67 records, and 29 standardized factors. Twenty-eight studies contributed 29 poolable estimates. Diagnostic delay (HR 1.401, 95% CI 1.077–1.822) and psychosocial stress (HR 1.237, 1.019–1.501) were positively associated with cancer-specific mortality. The particulate-matter estimate was highly heterogeneous (HR 1.427, 1.075–1.894; I^2=98.7%). The counterfactual baseline was 997.2 registered deaths (95% UI 834.4–1189.3). Under the no-attenuation upper-bound assumption of g=1.00, the primary six-factor model estimated 173.5 additional registered deaths (90.9–286.5). Across g=0.35–1.00, the increment ranged from 60.7 to 173.5 deaths. A flat-rate baseline sensitivity produced 127.8 additional deaths (65.5–215.0). Exploratory addition of particulate-matter exposure increased the estimate to 239.8 deaths (131.2–391.6).

Conclusion: War-related cancer factors were concentrated in health services and systems. Diagnostic delay and psychosocial stress showed positive pooled associations, while particulate matter remained exploratory. The estimated increments are conditional scenarios rather than observed or directly war-attributable deaths and depend on assumptions about baseline trends, exposure mapping, effect transport, overlap, and pathway coverage.

Introduction

Protracted war can simultaneously disrupt health-care facilities, transportation, referral, diagnosis, staffing, patient–provider communication, and living environments. Because patients with cancer depend heavily on continuity of care, pathological examination, surgery, radiotherapy and chemotherapy, and symptom control, shocks to the health system may affect their survival through multiple pathways[1]. However, in settings without complete cancer registration and individual follow-up, directly observing cancer-specific mortality during war is difficult. Reliance on hospital cases alone may also omit people who could not obtain care, were evacuated, or died without registration, limiting accurate assessment of the cancer burden[2].

Cancer care in conflict-affected settings is a problem of substantial and growing scale. Large populations of patients with cancer live in or are displaced from conflict zones such as Ukraine, Sudan, Syria, and Gaza, where treatment capacity, referral systems, and continuity of care have been severely disrupted[1,3]. Existing estimates of war-related cancer mortality, however, have mostly modelled a single pathway—typically treatment delay or interruption—and may therefore undercount the broader mortality burden[4]. In war settings, risks are not confined to the treatment process: health-care access, diagnostic capacity, workforce availability, patient–provider communication, psychosocial stress, and environmental exposures may all deteriorate simultaneously and act through shared care pathways.[5] These mechanisms can compound one another, while simply multiplying factor-specific effect estimates or adding their death increments may double-count shared pathways. A framework that systematically identifies the full set of war-related factors and then evaluates their individual and joint contributions is therefore needed. This study was designed as a direct response to that gap, and to the broader question of how health-system collapse beyond treatment interruption translates into cancer mortality risk.

Accordingly, this study first used a systematic review to identify factors associated with increased mortality among individuals with health conditions during war, standardized and classified these factors, and extracted those relevant to patients with cancer. Meta-analyses were then conducted for factors with evidence on cancer-specific mortality or survival. To apply this framework, we used prewar registered cancer deaths and population data for Gaza to extrapolate a 2023 no-war counterfactual baseline and combined this baseline with wartime exposure data in Monte Carlo simulations to estimate the change in deaths associated with each factor. Gaza is a relevant application setting because it has long depended on referrals and has faced constraints on medicines and equipment as well as barriers to cross-border movement[6]. After October 2023, the conflict further disrupted local cancer services, making access to continuous care more difficult[3]. Although Gaza is used here as the application setting, the factor map and scenario framework are intended to be transferable to other conflict settings. On this basis, the existing treatment delay or interruption factor was incorporated, co-exposure and shared pathways were handled explicitly, and a multifactor joint scenario was constructed to inform understanding of the potential effects of war on patients with cancer and the development of strategies to restore cancer services.

Materials and Methods

Study Design and Staged Analytical Framework

This study used a staged evidence-synthesis and scenario-modeling design. In the first stage, factors associated with increased mortality among individuals with health conditions during war were identified systematically, and a standardized factor database was established. In the second stage, a cancer-patient factor subset was formed from this database. In the third stage, quantifiable factors were selected on the basis of cancer-specific mortality or survival outcomes, and factor-specific meta-analyses were completed. In the fourth stage, the Gaza registry trend was used as a common counterfactual baseline. Six factor-specific scenarios were first evaluated. A, D, H, P, and C were then combined with the previously estimated treatment delay or interruption parameter T to construct the primary six-factor joint model. Because E was supported only by an indirect single-month exposure proxy, it was added only in an exploratory seven-factor extension[4]. The upstream systematic review defined the scope of the factors, the downstream meta-analyses estimated their effect sizes, and the scenario model estimated possible changes in registered deaths under explicit exposure-mapping and structural assumptions. These three components were not interpreted as equivalent.

In the second layer, A, D, H, P, and C were combined with T to form the primary six-factor joint scenario. E was excluded from the primary joint

model because its proxy covered only October 2023, was derived from stations outside Gaza, and was inconsistent in direction with the satellite-based alternative. E was added only in an exploratory seven-factor extension. The outcome for T was overall survival or all-cause mortality, and T was explicitly treated as an endpoint proxy.

Systematic Search and Study Selection for War-Related Factors

Search strategy and study selection

On August 12, 2026, we systematically searched four databases—PubMed, Embase, Cochrane Library, and Web of Science—using variants of terms such as “Armed Conflicts” and “Death” (for the detailed search strategy, see **Supplementary Materials, Section 1: Retrieval Strategy 1**).

The articles retrieved by the two researchers through the systematic search were first screened by title and abstract; disagreements were resolved through discussion until consensus was reached. The inclusion criteria for this screening stage were as follows:

Both of the following criteria had to be met:

1. Related to war
2. Must mention disease, i.e., the disease had to be related to war

The articles that were subsequently included were screened by full-text review. The inclusion and exclusion criteria are provided in **Supplementary Materials, Section 2**.

Data Extraction, Factor Standardization, and Quality Control

Data extraction: Data extraction was likewise performed independently and in duplicate by two reviewers, with disagreements resolved through discussion and consensus. Data were extracted using a predesigned data extraction form. The items extracted were: first author, year of publication, DOI/PubMed ID/link, name of the war/conflict, country/region, study period, study subjects/diseased population, type of study subjects, disease, Raw Factor name, evidence from the original text, and PDF page order. Country/region: Enter the region corresponding to the study/event or the geographic scope explicitly described in the article. The study region must not be inferred solely from the authors’ affiliations. Raw Factor name: Enter the original wording of the corresponding factor in the article, or a faithful and concise factor name taken from the original text; in principle, retain the English wording of the factor. Disease: Enter the disease or injury based on the information explicitly provided in the article. Multiple factors in a single article: When a single article reports multiple factors that meet the criteria:

Each independent factor should be entered on a separate row. All rows should use the same article-level information, such as article ID, DOI/PubMed ID/link, first author, and year. Multiple repeated pieces of evidence for the same factor should in principle be merged to avoid double counting.

Raw-Factor Standardization: This study standardized the original factors extracted from the literature using an item classification system and a controlled coding approach guided by an international framework; the standardization process is illustrated in **Supplementary Materials, Section 3: Figure 1**. The classification system consists of three data levels: “Primary Category,” “Standardized Factor Name,” and “Original Factor Name.” The primary category denotes the main analytical domain to which a standardized factor belongs; the standardized factor name serves as the uniform coding unit for factor aggregation and frequency counts; and the original factor name preserves the specific wording obtained during the literature extraction stage.

Method for Establishing Primary Categories: This study organized the original factors using an item analysis classification system guided by international frameworks. First, the four technical sectors of the *Sphere Handbook 2018*[7] —Health; Water Supply, Sanitation and Hygiene; Food Security and Nutrition; and Shelter and Settlement—were adopted as the initial classification framework. The research team then systematically compared all unique original factors extracted from the literature against this initial framework on an item-by-item basis and identified factors that could not be adequately covered by the four technical sectors. For factors related to health services, health workforce, medical products, medical equipment, health financing, and governance, further reference was made to the WHO Health System Framework[8] and the WHO HeRAMS[9]; for factors related to population displacement, hazard exposure, and disruption of critical infrastructure and essential services, reference was made to the terminology of the WHO Health Emergency and Disaster Risk Management[10], the UNDRR Sendai Framework Terminology[11], and the UNDRR/ISC Hazard Information Profiles[12]; for factors related to the economy, livelihoods, governance, social support, and rights, reference was made to the WHO Social Determinants of Health Framework[13] and the Sphere Protection Principles. (The formation pathway for each primary category is presented in **Excel Table 1, sheet 1**.) An independent definition record was established for each primary category, including the category name, operational definition, inclusions, exclusions, main international references, and boundaries with other primary categories (see **Excel Table 1, sheets 2 and 3**).

Method for Establishing the Standardized Factor Codebook: The research team first compiled all unique original factors (the rules for extracting unique original factors are provided in **Supplementary Materials, Section 4**) and, taking into account each factor’s direct target, state, primary mechanism of action, and position in the causal process, established candidate standardized factors. For standardized factor names, priority was given to standardized terminology from authoritative sources such as WHO, Sphere, UNDRR, or MeSH that corresponds closely to the study concepts; when international sources provided only basic concepts but lacked a complete risk factor expression, the research team developed project-specific standardized names without altering the core meaning of the original factors (see **Excel Table 2**). The conceptual definition and naming of standardized factors were informed by the terminology work principles of ISO 704 (https://www.iso.org/standard/79077.html). A complete codebook entry was established for each standardized factor, including the standardized factor name, operational definition, inclusion criteria, exclusion criteria, examples of mappable original factors, examples of non-mappable factors, term source type, and international references.

The management of the standardized factor vocabulary and mapping relationships was informed by the controlled vocabulary principles of ISO 25964-1 (https://www.iso.org/standard/53657.html). Each standardized factor was assigned a unique name and Factor_ID, while the original factor expressions from the literature extraction stage were retained, and the mapping results from original factors to standardized factors as well as the basis for the mapping decisions were recorded. ISO 704 and ISO 25964-1 were used to guide term definition, name harmonization, and the management of mapping records; they did not directly provide the primary categories or the list of standardized factors used in this study.

The relationship between primary categories and standardized factor names is defined as a classificatory assignment. A primary category is not

a synonym of a standardized factor, nor is it interpreted as a broader semantic term for the standardized factor; likewise, a standardized factor is not interpreted as a narrower term of a primary category. Each standardized factor is assigned to one primary category according to its primary target, mechanism of action, and field of application. In the visualization, the lines between primary categories and standardized factors are intended solely to indicate this classificatory assignment and do not represent strict semantic containment, causal sequence, or ontological relationships.

Quality Control: Two researchers independently coded all unique original factors based on the frozen primary category definition table and the standardized factor codebook. During the independent coding stage, the two researchers separately determined the primary category to which each original factor belonged, the corresponding standardized factor, and the mapping relationship, without viewing each other's judgments. After completing independent coding, the two researchers compared the results item by item. Items for which both the primary category and the standardized factor were consistent were adopted directly; items with disagreements were discussed by the two researchers, who jointly reviewed the original articles, the codebook, and relevant international reference materials. Items were adopted after consensus was ultimately reached through discussion (the mapping records of the two researchers are provided in **Excel Table 3**). Mapping Principles: A standardized factor could correspond to multiple original factors, provided that these original factors met the operational definition and inclusion criteria predefined for that standardized factor and did not meet its exclusion criteria. Specific drug, specialty, population, or disease information was retained in the original factor field; therefore, mapping to a unified standardized factor did not remove specific information obtained during the literature extraction stage.

Standardization was not aimed at minimizing the number of factors. In principle, factors describing different targets, states, or intervention steps were coded separately; for example, food shortage, food insecurity, hunger, and malnutrition were treated separately.

Identification of the Cancer-Patient Factor Subset

Within the standardized factor database, records potentially involving patients with malignant neoplasms were identified by starting with the disease and study-population fields. Article titles, abstracts, or full texts were then reviewed for each record to confirm whether the study population consisted of patients with cancer. At this point, the cancer-patient factor subset and the standardized factors within it were considered established. Whether effect-size studies had been retrieved or whether their effect estimates could be included in a meta-analysis played no part in defining this subset.

The frequency with which a factor appeared in the cancer-patient subset was used only to describe its coverage in the literature and did not indicate effect magnitude or causal strength. After the subset had been established, its factors proceeded to the next stage of effect-estimate retrieval. A factor remained in the cancer-patient factor subset even if no relevant effect-estimate study was retrieved or if all retrieved studies were excluded after title-and-abstract or full-text screening; it simply did not proceed to the subsequent meta-analysis or quantitative model. Previous research had already provided results for T, so its meta-analysis was not repeated in this study; T was used only in the subsequent joint model.

Systematic Review and Meta-Analysis of the Effects of War-Related Factors on Survival or Mortality Among Patients with Cancer

After the cancer-patient factor subset had been established, the research team searched for each factor in the subset on 13 September 2026. For each factor, its standardized name, original names, and synonyms were combined with terms for cancer populations and cancer-specific mortality or survival. PubMed, Web of Science, Embase, and the Cochrane Library were searched separately for evidence of effects on cancer-specific mortality or cancer-specific survival. The meta-analysis was registered in PROSPERO (CRD420261539143) and followed the PRISMA 2020 statement[14]. Two reviewers independently performed study screening, data extraction, and quality assessment. Disagreements were resolved through discussion and, when necessary, adjudication by a third reviewer. For each factor, the final set of studies was determined through retrieval, deduplication, title-and-abstract screening, full-text assessment, and application of the prespecified inclusion and exclusion criteria (see **Supplementary Materials, Section 2: Inclusion and Exclusion Criteria 2**). No relevant study was identified for some factors. For other factors, candidate studies were retrieved but none remained after screening because the study population, exposure definition, or outcome was ineligible; an HR and 95% CI were unavailable and the effect estimate could not be reconstructed; or cohorts were duplicated, among other reasons (for the inclusion process and reasons for non-inclusion for each factor, see **Supplementary Materials, Section 3: Figure 2**). Six factors with eligible studies were ultimately retained. Health workforce loss and Health workforce loss or shortage were combined as Health workforce loss or shortage (for the search strategies for each factor, see **Supplementary Materials, Section 1: Retrieval Strategy 2**; for the reasons why factors were not included, see **Supplementary Materials, Section 3: Figure 2**).

Risk of bias was assessed at the outcome level using the 24 March 2024 version of ROBINS-E[15]. The overall judgment was determined by the most serious domain.

Meta-analysis: Inverse-variance weighting was performed on the log-HR scale. If the lower and upper limits of a reported 95% CI were L and U, respectively, the standard error was calculated as follows:

$$SE[ln(HR)] = [ln(U) - ln(L)]/3.92$$

Because the included studies differed in populations, cancer sites, and exposure definitions, a single common effect was not assumed. Random-effects meta-analysis was therefore used as the primary model for every factor, irrespective of I^2. Between-study variance (τ^2) was estimated by restricted maximum likelihood (REML), and conventional 95% confidence intervals for the pooled effects were calculated using a normal approximation. Cochran's Q, I^2, and τ^2 were reported. When at least three studies were available, a 95% prediction interval was calculated under the random-effects model. Fixed-effect estimates were retained as model-sensitivity analyses. For patient–provider communication barriers (C), only two studies were available and τ^2 was estimated as 0; the random-effects estimate was numerically identical to the fixed-effect estimate, but τ^2 was considered imprecisely estimated and the result was interpreted cautiously. Publication-bias testing was not performed when fewer than 10 studies were included for a factor; Egger's or Begg's test was not performed when only two studies were available. Results from the primary and sensitivity models are presented in **Supplementary Materials, Section 5, Tables 2**.

Studies of particulate matter reported effects for different concentration increments. Under a log-linear assumption, these effects were standardized to an HR per 10 μg/m³ increase:

$$HR_{10} = HR_{\Delta}^{10/\Delta}$$

Here, Δ denotes the concentration increment corresponding to the HR in the original study. This conversion depends on a log-linear relationship. When an original study reported a nonlinear association or when an estimate for a smaller concentration increment was extrapolated to 10 μg/m³, this issue was addressed separately in sensitivity analyses and as a limitation. If the health-workforce evidence included both Cox cause-specific HRs and Fine–Gray subdistribution HRs, they were pooled only in an exploratory analysis on a common log-HR scale, with explicit acknowledgment that they are not fully equivalent.

Counterfactual Baseline of Registered Cancer Deaths in Gaza in 2023

Baseline data comprised the numbers of registered cancer deaths in Gaza from 2016 to 2022 reported in the annual reports of the Palestinian Ministry of Health (see **Supplementary Materials, Section 5: Table 1**), together with the corresponding mid-year population estimates and the 2023 mid-year population published by the Palestinian Central Bureau of Statistics[16,17]. Historical registered deaths were not adjusted for under-registration. The baseline used in the present analysis differs from that reported in the companion study because the two analyses used different source series and reconstruction strategies. The companion study derived a registry-equivalent Gaza baseline indirectly from national GBD estimates and West Bank registry data and examined Gaza-only extrapolations based on 2019 – 2022 as sensitivity analyses. In contrast, the present study directly fitted annual Gaza registered cancer deaths compiled from Ministry of Health reports for 2016 – 2022. Consequently, the GBD-residual reconstruction used in the companion study and the direct Gaza registry series used here produced different apparent temporal patterns and different 2023 counterfactual baselines. These estimates were therefore not expected to coincide and were compared only after distinguishing the registered-death scale from the total-death scale. The longer window was selected to stabilize estimation from a short annual series, while recognizing the unresolved inconsistencies in the 2017 – 2018 data and a possible reporting discontinuity associated with the reorganization of oncology services in late 2021.

The estimand was the expected number of registered cancer deaths in 2023, assuming that the prewar cancer-death registration process and the 2016–2022 trend in the registered cancer mortality rate continued through 2023. This counterfactual baseline does not represent the number of deaths actually registered in 2023 or the true total number of cancer deaths after adjustment for under-registration.

Let (Y_t) denote the number of registered cancer deaths in year (t), let (P_t) denote the corresponding mid-year population, and define $(x_t = t - 2016)$. The primary analysis used a Poisson log-linear trend model with the logarithm of population as an offset:

$$Y_t \sim Poisson(\mu_t)$$
$$\log(\mu_t) = \alpha + \beta x_t + \log(P_t)$$

Here, (α) is the intercept, (β) represents the annual change in the registered cancer mortality rate on the logarithmic scale, and $(\log(P_t))$ is the population offset with its coefficient fixed at 1. This model estimates the temporal trend in the registered cancer mortality rate while allowing the expected number of registered deaths to vary with population size.

A Pearson dispersion parameter was used to assess extra variation in annual death counts relative to the Poisson distribution assumption:

$$\hat{\phi} = \frac{\sum_t (Y_t - \hat{\mu}_t)^2 / \hat{\mu}_t}{n - p}$$

Here, (n) is the number of annual observations and (p) is the number of model parameters. When $(\hat{\phi} > 1)$, the coefficient covariance matrix from the Poisson model was multiplied by $(\hat{\phi})$:

$$\widehat{Var}_{\text{adj}}(\hat{\alpha}, \hat{\beta}) = \hat{\phi}\, \widehat{Var}_{\text{Poisson}}(\hat{\alpha}, \hat{\beta})$$

The Pearson dispersion correction does not change the model coefficients or the point estimate of the counterfactual baseline. It is used only to reflect extra variation in the historical series and to adjust parameter uncertainty accordingly.

The point estimate of the counterfactual number of registered cancer deaths in 2023 was calculated as follows:

$$D_{0,2023} = P_{2023} exp\left(\hat{\alpha} + 7\hat{\beta}\right)$$

Here, (P_{2023}) is the mid-year population of Gaza in 2023, and 7 denotes the interval between 2023 and 2016, the first year of the model. Uncertainty in the trend parameters was propagated through the Monte Carlo simulation described below.

Temporal-order testing used an expanding-window approach. Data from 2016–2017 were first used to predict 2018, after which the training window was expanded by one year at a time until data from 2016–2021 were used to predict 2022, yielding five one-step-ahead prediction folds. Prediction error, absolute error, and absolute percentage error were calculated for each fold, and mean absolute error, root mean square error, and mean absolute percentage error were summarized. Because the first fold contained only two training observations, exactly sufficient to estimate the intercept and annual trend parameters, dispersion could not be estimated reliably. This test was therefore used only to assess the temporal consistency of one-step point predictions and was not considered sufficient external validation.

To assess the sensitivity of the counterfactual baseline to model structure, four additional scenarios were specified: a standard Poisson model without Pearson dispersion correction, a linear trend model for registered death counts, a log-linear trend model for the crude registered cancer mortality rate, and a flat-rate scenario based on the arithmetic mean of the exact crude registered cancer mortality rates observed during 2019–2022. For the flat-rate scenario, the mean rate was multiplied by the 2023 mid-year population. Uncertainty in the mean rate was approximated using the between-year standard error of the four annual rates, and 100,000 normally distributed rate draws were propagated to the 2023 population. The flat-rate scenario was prespecified as a conservative structural sensitivity and did not replace the primary 2016–2022

Pearson-dispersion-corrected Poisson trend model. All scenarios used the same target population for 2023.

To facilitate scale-matched comparison with the total-death estimates reported in the companion study and the Gaza Mortality Survey-derived external approximation, we additionally conducted an illustrative registration-completeness conversion. Let$c$denote assumed registration completeness. For each fixed value of c, the implied total number of deaths and the implied total-death increment were calculated as $D_{\text{total}} = D_{\text{registered}}/c$ and $\Delta D_{\text{total}} = \Delta D_{\text{registered}}/c$, respectively. We examined completeness values of 0.70, 0.775, 0.80, and 0.85, corresponding to the range used in the companion study. Because c was treated as a fixed scale-conversion parameter, the relative increase from baseline was unchanged. This analysis was intended only to reconcile reporting scales and was not treated as a new primary model. It assumes that the selected completeness value applies equally to the counterfactual and wartime scenarios and therefore does not account for a possible wartime deterioration in death registration.

Factor-Specific Scenario Models for the Six Factors

For factor i, the number of registered deaths under the scenario and the paired increment relative to the common baseline were defined as follows:

$$D_{\mathrm{i}} = D_0 \times [1 + (m/12) \times f_{\mathrm{i}} \times g \times (E_{\mathrm{i}} - 1)]$$
$$\Delta D_{\mathrm{i}} = D_{\mathrm{i}} - D_0$$

Here, m=3 months. For A, D, H, P, and C, E_i=HR_i; for particulate matter, $E_E = HR_{10}^{\Delta x/10}$, with Δx=4.1 μg/m³ in the exploratory factor-specific analysis. The preceding factor-specific equation linearly scales the excess component of the literature-based HR, HR−1, by the duration of exposure as a proportion of one year and by the effective affected-burden fraction. An HR is an instantaneous hazard ratio and is not equivalent to a three-month cumulative risk ratio. In the absence of individual survival curves, baseline hazards, and competing-risk data, this linear relationship is a transparent but simplified approximation.

Wartime mapping parameters: All six factor-specific scenarios began from the same common baseline, with only one newly analyzed factor entered at a time to show the conditional signal associated with each pathway. The factor-specific results cannot be added to one another.

HRs reported in the literature describe relative instantaneous hazards under the definitions used in the original studies, whereas wartime data usually provide proportions relating to personnel, patients, or environmental monitoring. To link these two types of data, an effective affected-burden fraction, f, was defined for each factor. The value of f is not an etiologic attributable fraction and need not equal the total patient exposure prevalence. Formally,$f$is defined as the effective proportion of the counterfactual registry baseline that experiences the **wartime increment** in a given factor—that is, exposure above the prewar counterfactual level. Because $D0$ already incorporates prewar permit delays, diagnostic delay, psychosocial distress, and other prewar constraints, applying $f$to the total exposed proportion would count prewar exposure twice. Where only total wartime exposure proportions were available, we used them as proxies for the wartime increment. This is equivalent to treating prewar exposure as the reference level or as negligible relative to the wartime change; it may overstate the incremental exposed fraction and is therefore best interpreted as an upper-bound mapping. This assumption was examined through the prespecified $f$and g sensitivity analyses and is acknowledged in the Limitations. The realization coefficient, g, describes the proportion of the excess relative hazard reported in the literature that is realized within the three-month window. The primary upper-bound scenario used g=1.00, indicating no temporal attenuation of the excess relative hazard within the three-month window. This is an upper-bound modeling choice and does not establish that all long-term effects would occur within three months. Sensitivity analyses used values of 0.35, 0.50, and 0.65. Under the current specifications, A, P, and C were proxied mainly by proportions among patients or respondents; H was proxied by the proportion of personnel unavailable; and D was based on the shortfall in diagnostic activity and a range anchored to authoritative reports, with 0.75 used as the data-anchored central assumption. The primary definition of C was Very poor+Poor (197/658), with Fair excluded; the previous definition that included Fair was used only in a definitional sensitivity analysis. No direct continuous monitoring data from Gaza were available for E. Therefore, Δx was proxied only by the year-on-year difference in October PM2.5 between 2023 and 2022 at a neighboring station. This proxy did not cover November or December, so E was explicitly treated as exploratory. Accordingly, E was excluded from the primary joint model and was added only in an exploratory seven-factor extension. None of these values was directly observed as the fraction of a conditional scenario change in registered cancer deaths or as a causal wartime increment (for the search history, inclusion and exclusion criteria, and calculation process for the wartime mapping parameter f for each factor, see **Supplementary Materials, Section 6: Part I**; for the f values and primary-analysis specifications for each factor, see **Supplementary Materials, Section 5: Table 3**).

Primary Six-Factor Joint Exposure and Pathway Model and Exploratory Addition of Particulate Matter

The primary joint-effects model combined health-care access barriers, diagnostic delay, health workforce loss or shortage, psychosocial stress, and patient–provider communication barriers with treatment delay or interruption from the preceding study. Particulate-matter exposure was excluded from the primary joint model and was added separately in an exploratory seven-factor extension. The numbers of additional deaths under the individual-factor scenarios were not directly summed, nor were the factor-specific HRs directly multiplied for all patients, because different factors may occur in the same patient and may affect mortality through treatment delay or interruption. Direct summation or multiplication could double-count the same patients and shared pathways of action. **Table 1** summarizes the parameters for the six factors in the primary joint model and the particulate-matter parameter used only in the exploratory extension.

Table 1. Parameters used in the primary six-factor joint model and the exploratory particulate-matter extension

Factor	Pooled HR (95% CI)	f (primary; sensitivity range)	Overlap with T: P(T|factor) or equivalent	Source / basis
A	1.127 (0.938–1.353)	0.20 (0.18–0.22)	P(T|A) = 1.000 (definitional nesting)	Meta-analysis (this study); OCHA Flash Update 14[18]、WHO Health Access Monthly Report 2023-07[19]、Bouquet 2021[20]
D	1.401 (1.077–1.822)	0.75 (0.50–1.00)	P(T|D) = 0.827 (0.805–0.849)	Meta-analysis (this study); MoH Annual Report 2022[21], PCHR 2024/2025[22,23], WHO/OCHA Data[24,25], Gade et al. 2×2 table[26]
H	1.013 (0.941–1.090)	0.70 (0.50–0.90)	P(T|H) = 0.920 (0.750–0.950)	Meta-analysis (this study); WHO/MoH briefing[27]、WHO EMRO[28]、

P	1.237 (1.019–1.501)	0.80 (0.50–0.94)	P(T|P) = f_T = 0.75 (assumed independent)	PCHR[22, 23]、Gaza cancer care mapping[29]
E, exploratory extension only	1.427 (1.075–1.894)	f = 1.00 (area-level exposure)	Continuous exposure; no binary overlap	Meta-analysis (this study); Hejaz 2025[30]、Brugger 2025[31]、Rihani 2025[32]、Albelbeisi 2025[33]、Abu-Odah 2022[34]
C	1.352 (0.978–1.869)	0.299 (0.100–0.549)	P(T|C) = 0.858 (0.829–0.884)	Meta-analysis (this study); Ashkelon Monitoring Report 2023/2022[35,36], IPC[37], UNEP[38], Mohamadi 2025[39]
T	1.085 per 4 weeks (1.051–1.120); 1.277 at 12 weeks (1.161–1.405)	0.75 (0.50–1.00)	Reference factor	Meta-analysis (this study); Asfour 2025[40]、Elsous 2023[41]、Tamirat 2025: C–T Overlap[42]
				SSRN preprint (Luo et al. 2025)[4]

Notes: HR, hazard ratio; f, effective affected-burden fraction; T, treatment delay or interruption. For the exploratory seven-factor extension, the HR for E was expressed per 10 μg/m³ and converted to the selected concentration increment Δx. E was not included in the primary six-factor joint model. P(T|P) is set equal to f_T because psychosocial stress is assumed independent of T. The T parameter was derived from a previously posted SSRN preprint and was used here as an external proxy, not as a newly estimated result of this study. Full derivations of the wartime mapping and overlap parameters are provided in Supplementary Materials, Section 6; the T-only reference and joint-model sensitivity results are reported in Supplementary Tables S4A, S5A–S5D, and S10.

In the primary joint model, A, D, H, P, C, and T were defined as binary states, yielding 64 mutually exclusive combinations. The effective affected-burden fraction for each factor served as its marginal weight. E was not included in these primary-model combinations. In the exploratory seven-factor extension, particulate-matter exposure was added separately as a continuous area-level multiplier.

Particulate-matter exposure was treated as a continuous area-level exposure; the pooled HR per $(10\,\mu g/m^3)$ increase was converted to the relative effect corresponding to the actual exposure increment (Δx) using the following equation:

$$R_E^{(s)} = \left(HR_{E,10}^{(s)}\right)^{\Delta x/10}$$

The effect of treatment delay or interruption was based on the HR per 4-week delay and converted for the 12-week wartime observation window:

$$R_T = HR_{T,4w}^3$$

This conversion assumes that the log-HR increases linearly across three consecutive four-week periods and does not represent a directly observed 12-week effect.

Because the original evidence for treatment delay or interruption primarily used overall survival or all-cause mortality outcomes, whereas the five non-treatment factors in the primary joint model used cancer-specific mortality outcomes, we assessed this difference using the endpoint-transport coefficient λT. A value of λT=1 indicates complete endpoint transport, λT=0.5 indicates retention of only 50% of the log effect, and λT=0 indicates no transport of the direct mortality effect of treatment delay or interruption. All three settings were reported in parallel, and each represents a conditional endpoint-transport scenario rather than a validated cancer-specific causal effect. Accordingly, the endpoint-transported effect of treatment delay or interruption used in the joint model was defined as:

$$R_T^* = R_T^{\lambda_T}$$

All subsequent joint-model and treatment-interruption-only calculations used R_T^*, rather than the unmodified R_T.

The joint distribution was constructed around treatment delay or interruption (T). First, based on the marginal weight of each factor and its evidence-calibrated degree of overlap with (T), we calculated:

$$P(i = 1 \mid T = 1) \quad and \quad P(i = 1 \mid T = 0)$$

Conditional on (T), the remaining factors were assumed to be mutually independent, and the weights of the 64 combinations were calculated accordingly. The conditional overlap parameters between each factor and treatment delay or interruption, evidence sources, calculation methods, and sensitivity ranges are detailed in **Supplementary Materials, Section 6**: **Part II**.

To avoid double-counting the same pathway, once treatment delay or interruption had occurred, the incremental effects of health-care access barriers, health workforce loss or shortage, and patient–provider communication barriers were considered to be covered by the treatment-interruption pathway; psychosocial stress retained its full independent effect, whereas diagnostic delay retained only a prespecified residual effect. The definition and basis for the residual effect of diagnostic delay, together with sensitivity analyses using different residual proportions, are detailed in **Supplementary Materials, Section 6**: **Part II**.

Let $\mathcal{B} = \{A, D, H, P, C\}$ denote the set of five binary non-treatment factors. For each $i \in \mathcal{B}$, let R_i denote the pooled relative effect, define $p_{i0} = P(i = 1 \mid T = 0)$ and $p_{i1} = P(i = 1 \mid T = 1)$, and let$\kappa_i$ denote the proportion of the log effect of factor $i$retained after treatment interruption occurred. Particulate-matter exposure E was applied separately as a continuous area-level multiplier and was therefore not included in the product over $\mathcal{B}$. The conditional joint relative effect among those without treatment interruption was:

$$R_0 = R_E \prod_{i \in \mathcal{B}} [1 + p_{i0}(R_i - 1)]$$

The conditional joint relative effect among those with treatment interruption is:

$$R_1 = R_E R_T^* \prod_{i \in \mathcal{B}} \left[1 + p_{i1}\left(R_i^{\kappa_i} - 1\right)\right]$$

The two conditional effects were then weighted by the effective affected-burden fraction (f_T) for treatment delay or interruption to obtain the overall joint relative effect:

$$R_J = (1 - f_T)R_0 + f_T R_1$$

This calculation is equivalent to a weighted average of the relative effects across the 64 mutually exclusive combinations and does not imply that every patient experienced all factors simultaneously. The probabilities of the 64 mutually exclusive combinations under the primary joint structure are provided in **Supplementary Materials, Section 5: Table 4**.

Using registered cancer deaths and the corresponding mid-year population in Gaza from 2016 to 2022, we fitted a Poisson log-linear trend model corrected for Pearson dispersion and used it to estimate the 2023 counterfactual baseline (D_0) of registered cancer deaths in the absence of war. For a war-impact window of $(m = 3)$ months, with (g) denoting the risk-realization coefficient, the annual number of registered cancer deaths under the joint scenario is:

$$D_J = D_0\left[1 + \frac{m}{12}g(R_J - 1)\right]$$

The increase in registered deaths relative to the no-war counterfactual baseline is:

$$\Delta D_J = D_J - D_0$$

For model-reduction checks and paired comparison, the treatment-interruption-only reference was calculated using the endpoint-transported treatment effect:

$$R_{T,\text{only}} = 1 + f_T(R_T^* - 1)$$

$$D_{T,\text{only}} = D_0\left[1 + \frac{m}{12}g\left(R_{T,\text{only}} - 1\right)\right]$$

$$\Delta D_{J-T} = D_J - D_{T,\text{only}}$$

The paired difference ΔD_{J-T} was calculated within each Monte Carlo iteration and therefore cannot be obtained by directly subtracting the two marginal medians.

Monte Carlo Sampling and Uncertainty Propagation

Monte Carlo simulation was used to propagate the statistical uncertainty in the no-war counterfactual baseline and the pooled effect estimate for each factor. All analyses used 100,000 parameter iterations with the random seed set to 20260921 to ensure reproducibility.

At iteration (s), the intercept $(\alpha^{(s)})$ and annual trend coefficient $(\beta^{(s)})$ were drawn jointly from a bivariate normal distribution centered on the Poisson model coefficient estimates, with the Pearson-dispersion-corrected variance–covariance matrix used as the covariance matrix. This sampling preserved the correlation between the two regression coefficients. The iteration-specific counterfactual number of registered cancer deaths in the absence of war was then calculated using the 2023 mid-year population:

$$D_0^{(s)} = P_{2023}exp\left(\alpha^{(s)} + 7\beta^{(s)}\right)$$

The simulation propagated parameter uncertainty in the estimated counterfactual mean and did not add an additional Poisson random count to the predicted mean.

For each included factor, the pooled HR was assumed to be approximately normally distributed on the log scale. If the pooled HR and its 95% confidence interval were $\hat{HR}_i$, L_i, and U_i, respectively, the log standard error and the value sampled at iteration s were, respectively:

$$SE_i = [ln(U_i) - ln(L_i)]/3.92;\ \ln(HR_i^{(s)}) \sim \mathcal{N}\left[\ln(\widehat{HR}_i), SE_i^2\right]$$

Because the meta-analyses of different factors did not provide covariances among the effect estimates, the factor-specific HRs were sampled independently. This sampling represents the statistical uncertainty in the pooled effect estimates and is not equivalent to the between-study predictive distribution from a random-effects meta-analysis.

At each iteration s, the particulate-matter effect was converted as

$$R_E^{(s)} = \left(HR_{E,10}^{(s)}\right)^{\Delta x/10}$$

The effect of treatment delay or interruption was converted to the 12-week observation window as

$$R_T^{(s)} = \left(HR_{T,4w}^{(s)}\right)^3,$$

and the endpoint-transported effect was then calculated as

$$R_T^{*(s)} = \left(R_T^{(s)}\right)^{\lambda_T},$$

with λ_T set to 1, 0.5, and 0. The iteration-specific values of $R_1^{(s)}$ and $R_{T,\text{only}}^{(s)}$ were calculated by substituting$R_T^{*(s)}$ for R_T in the corresponding equations.

The sampled $D_0{}^{(s)}$ and factor-specific HRs for A, D, H, P, and C, together with the transported treatment-delay or interruption effect, were entered into the primary six-factor joint model. The converted particulate-matter effect was added only in the exploratory seven-factor extension. Within each prespecified scenario, the effective affected-burden fractions, conditional overlap parameters, proportion of the residual effect of diagnostic delay, risk-realization coefficient, particulate-matter concentration increment, and endpoint-transport coefficient for treatment delay were held fixed and varied separately through discrete sensitivity analyses. The settings and supporting rationale for the conditional overlap relationships among factors and for the residual effect of diagnostic delay are provided in **Supplementary Materials, Section 6**.

The joint scenario and the reference scenario containing only treatment delay or interruption were simulated as a pair: the same counterfactual baseline and the same sampled treatment-delay effect were used within each iteration, and the difference in the number of deaths between the two scenarios was then calculated directly. The paired difference was summarized from the distribution of within-iteration differences, rather than by subtracting the marginal medians of the two scenarios.

The median of the 100,000 simulation results was used as the point estimate, and the 2.5th and 97.5th percentiles of the empirical distribution were used as the 95% uncertainty interval (95% UI). This interval primarily reflects statistical uncertainty in the counterfactual baseline trend parameters and the meta-analytic pooled effect estimates; structural uncertainties in the effective affected-burden fractions, co-occurrence structure, pathway coverage, risk-realization coefficient, and endpoint transport were reported for the primary joint model; particulate-matter exposure increments were assessed separately in the exploratory extension. All simulations were performed in Python 3.10.

Sensitivity Analyses and Program Verification

Factor-specific sensitivity analyses sequentially varied the baseline model, meta-analysis model, effective affected-burden fraction f, realization coefficient g, particulate-matter concentration increment Δx, and the definition of communication barriers C. Alternative baseline scenarios included a Pearson-dispersion-corrected Poisson rate trend, an ordinary Poisson rate trend, a linear trend in registered death counts, a log-linear trend in the crude registered mortality rate, and a flat-rate scenario based on the arithmetic mean of the exact 2019–2022 crude registered cancer mortality rates; fixed-effect results were used to assess the choice of meta-analysis model; prespecified low, primary, and high values of f were used for each factor; g was set to 0.35, 0.50, 0.65, and 1.00; particulate-matter Δx was set to 0, 0.5, 4.1, and 7.2 μg/m³, with additional factor-specific exploratory scenarios using a satellite-based alternative and household fuel smoke; and the old classification definition of C was evaluated using 197/658, 395/658, and 559/658. The primary joint model tested κD values of 0, 0.5, and 1; six overlap structures; full multiplicative and additive excess-risk bounds; λT values of 1, 0.5, and 0; all-low, primary, and all-high f values; g values of 0.35, 0.50, 0.65, and 1.00; fixed-effect estimates for A, D, H, P, and C; the previous definition of C; and five baseline scenarios. E was subsequently added only in exploratory extended-model scenarios using Δx values of 0.5, 4.1, and 7.2 μg/m³. Each scenario was run separately, and the 95% UI propagated only uncertainty in the trend and HR parameters within the corresponding fixed scenario. The satellite-based alternative and household fuel smoke were used only for factor-specific exploratory analyses of E and were not included in the current joint model. Full specifications are provided in **Supplementary Materials, Section 7: Supplementary Table S1**.

Trend extrapolation was assessed through an internal test using a chronologically expanding training window: beginning with the use of 2016–2017 data to predict 2018, the training period was extended by one year at a time until 2016–2021 data were used to predict 2022. For each fold, the predicted value, observed value, prediction error, absolute error, and absolute percentage error were recorded, and MAPE, MAE, and RMSE were summarized. Program verification checked whether the counterfactual baseline number of deaths, sampled HR/RR values, and wartime relative risks were all greater than 0 in every iteration; whether all numeric values were finite; whether a fixed random seed reproduced the output exactly; and whether formula constraints for probabilities, marginals, intersections, model reduction, annual scaling, and Shapley additivity could be independently recalculated and shown to hold. Paired increments in deaths with an uncertain direction were permitted to be below 0. Reporting followed the GATHER requirements for transparency in data sources, assumptions, sampling, and sensitivity analyses[43]; full methods and results are provided in **Supplementary Materials, Section 7:** Supplementary Tables S**2 and S3**.

Results

Systematic Review Screening and Map of War-Related Factors

A total of 21,938 records were independently identified by two researchers using a predefined search strategy in the databases. 1,123 reports were assessed for eligibility, and ultimately, 413 studies met the inclusion criteria for synthesis (See **Supplementary Materials, Section 3: Figure 3** for the PRISMA literature screening flowchart). Detailed information on article characteristics is provided in **Excel Table 4**.

A total of 1,341 valid factor records were included in this study. Following terminology harmonization and classification mapping, 263 factors were established and assigned to seven primary categories. Of these, 111 factors occurred at least twice, accounting for 1,189 factor records, or 88.7% of all valid records, and were therefore included in the two-level tree (See **Figure 1-A**). The remaining 152 factors occurred only once, accounting for 11.3% of all records; these factors were not displayed in the tree but were listed separately in the appendix under their respective primary categories (See **Supplementary Materials, Section 5: Table 5**). Both the primary categories and the standard factors within each category were ordered by descending frequency. By number of factor records, health services and systems accounted for 710 records (52.9%); food security and nutrition, 179 (13.3%); shelter, settlement, and population displacement, 141 (10.5%); protection, conflict, and hazardous exposures, 122 (9.1%); WASH, 91 (6.8%); the socioeconomic, governance, and rights environment, 59 (4.4%); and humanitarian access, transport logistics, and critical infrastructure, 39 (2.9%). The first three categories accounted for 1,030 records (76.8%) in total. These figures reflect the distribution of factors reported in the included studies and cannot be directly interpreted as population-attributable proportions or factor-specific risks.

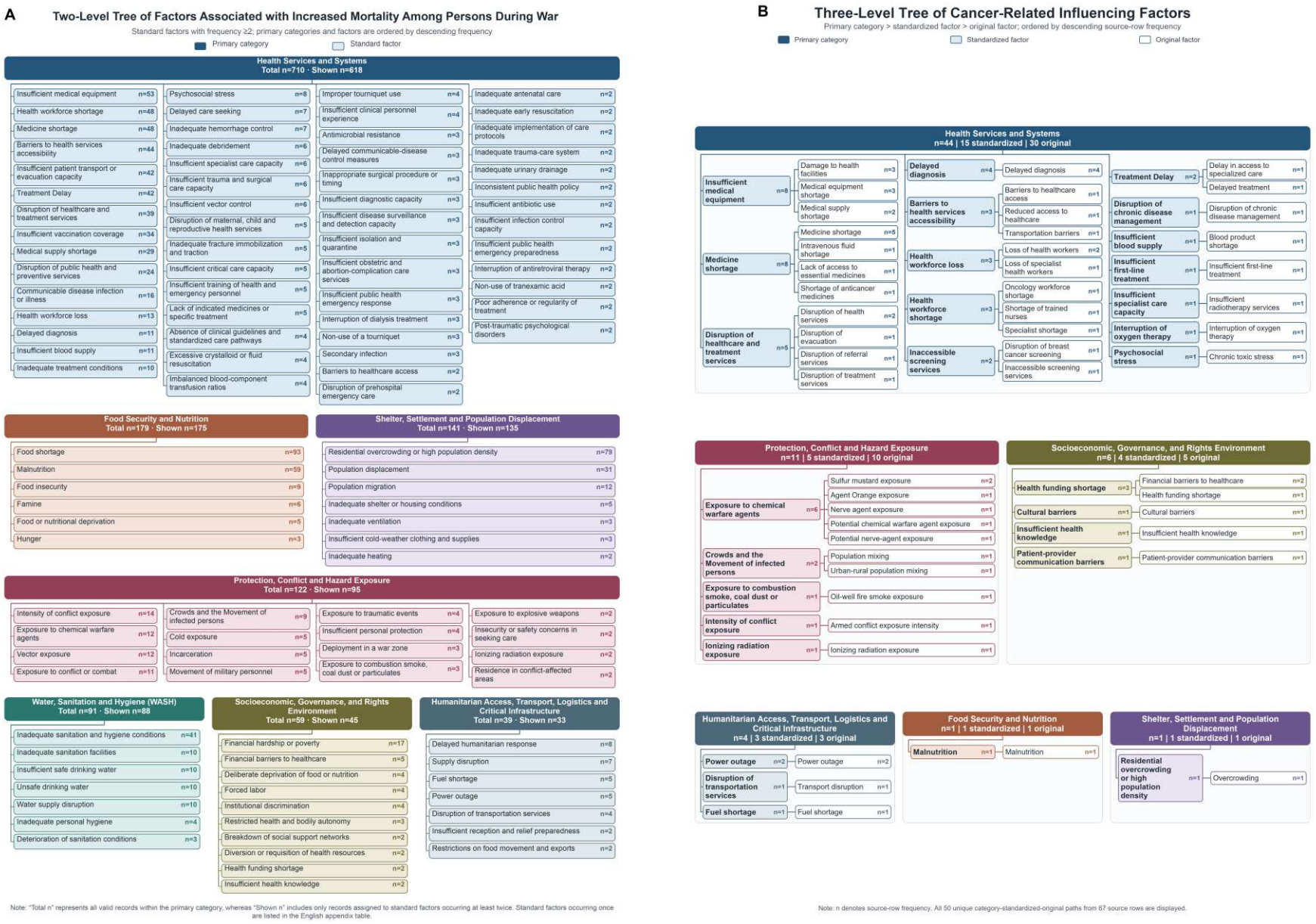


Figure 1. Hierarchical distribution of war-related factors associated with increased mortality and the cancer-related factor subset.

(A) Two-level tree showing primary categories and standardized factors reported at least twice across the included studies. Within each primary category, standardized factors are arranged in descending order of frequency. "Total n" represents all valid factor records assigned to that category, whereas "Shown n" represents records mapped to standardized factors with a frequency of at least two. Standardized factors reported only once are not displayed. (B) Three-level tree showing the primary category, standardized factor, and original factor for the cancer-related subset. All unique category–standardized factor–original factor mapping paths are displayed and ordered by source-row frequency. In panel B, *n* denotes the number of source rows, and the category headings report the total number of source rows and the numbers of standardized and original factors. Colors distinguish the primary categories; dark boxes denote primary categories, lightly shaded boxes denote standardized factors, and white boxes denote original factors. Connecting lines indicate classification and mapping relationships rather than causal pathways. WASH, water, sanitation and hygiene.

Cancer-Patient Factor Subset and Effect-Size Screening Results

The cancer-patient subset included 23 studies, 67 factor records, 50 original factor names, and 29 standardized factors across six primary categories. Of these, the health services and systems category contained 44 records (65.7%) and represented the greatest concentration of evidence (**see Figure 1-B**). The most frequent standardized factors in the cancer-patient subset were medicine shortages and inadequate medical equipment (both n=8), followed by exposure to chemical warfare agents (n=6), disruption of medical and treatment services (n=5), and diagnostic delay (n=4). Health workforce loss or shortages, health funding shortages, health workforce loss, and health-care access barriers each occurred three times; treatment delay, lack of access to screening services, population crowding and movement of infected persons, and power outages each occurred twice; and all remaining standardized factors occurred once. After the cancer-patient factor subset had been identified, each factor was searched individually for studies reporting effects on cancer-specific mortality or survival. Following the search and screening, six factors—A, D, H, P, E, and C—ultimately entered the meta-analysis and factor-specific quantitative analyses. A, D, H, P, and C were subsequently included in the primary joint model, whereas E was retained only for the exploratory extension.

Cancer-Specific Effect Evidence and Pooled Results

ROBINS-E assessments showed that 2 of the 5 health-service-accessibility effects were at high risk of bias and 3 raised some concerns. For diagnostic delay, 1 effect was at high risk and 3 raised some concerns. All 7 health-workforce studies raised some concerns. For psychosocial stress, 3 studies were at high risk and 2 raised some concerns; for particulate matter, 5 were at high risk and 1 raised some concerns; and for communication barriers, 1 was at high risk and 1 raised some concerns. Because every factor was represented by fewer than 10 studies, publication-bias analyses were not performed. Egger's or Begg's tests were likewise not conducted for communication barriers, which were represented by only 2 studies (detailed quality-assessment results are provided in **Supplementary Materials, Section 5: Table 6**).

Ultimately, 28 studies contributed 29 poolable effect estimates. Random-effects REML models were used as the primary analysis for all six factors. The pooled HRs (95% CIs) were 1.127 (0.938–1.353) for health-care access barriers, 1.401 (1.077–1.822) for diagnostic delay, 1.013 (0.941–1.090) for health workforce loss or shortage, 1.237 (1.019–1.501) for psychosocial stress, 1.427 (1.075–1.894) for particulate matter, and 1.352 (0.978–1.869) for patient–provider communication barriers. For C, only two studies were available and τ^2 was estimated as 0; the

random-effects and fixed-effect estimates were therefore numerically identical, but the between-study variance remained imprecisely estimated. Fixed-effect estimates are reported as sensitivity analyses (detailed results are provided in **Table 2**, and a complete comparison of the primary and alternative meta-analysis models is provided in **Supplementary Materials, Section 5: Table 8**).

Table 2. Pooled cancer-specific effects of the six newly examined non-treatment factors

Factor	Studies/effect estimates	Primary model	Pooled HR (95% CI)	I^2(%)	τ^2	95% prediction interval
A Health-care access barriers	4/5[44-47]	Random-effects REML	1.127 (0.938–1.353)	84.1	0.0283	0.611–2.079
D Diagnostic delay	4/4[48-51]	Random-effects REML	1.401 (1.077–1.822)	54.9	0.0252	0.573–3.424
H Health workforce loss or shortage	7/7[52-58]	Random-effects REML	1.013 (0.941–1.090)	73.8	0.0067	0.804–1.277
P Psychosocial stress	5/5[59-63]	Random-effects REML	1.237 (1.019–1.501)	58.7	0.0255	0.680–2.248
E Particulate matter (per 10 μg/m³)	6/6[64-69]	Random-effects REML	1.427 (1.075–1.894)	98.7	0.0987	0.546–3.727
C Patient–provider communication barriers	2/2[70,71]	Random-effects REML	1.352 (0.978–1.869)	0	0	Could not be estimated reliably.

Note: HR>1 indicates that a less favorable factor was associated with a higher risk of cancer-specific mortality. Prediction intervals describe the distribution of effects across studies and were not used for Monte Carlo sampling.

Because C was represented by only two studies, τ^2 was imprecisely estimated and a prediction interval could not be estimated reliably.

Auxiliary Evidence for the Joint Structure

The Gaza permit study for A and T could support only the presence and magnitude of barriers and could not directly estimate P(T|A); P(T|A)=1 was therefore based on definitional nesting. For D and T, we used the four-cell table from Gade et al. for 418 patients: 129 with both D and T, 91 with D only, 48 with T only, and 150 with neither, yielding a crude OR of 4.4299 (95% CI 2.9064–6.7521). For H and T, we used an institution-level proxy from the Royal College of Radiologists, according to which 92% of 60 centers experienced radiotherapy delays due to workforce shortages. For C and T, we used the adjusted OR of 2.54 (1.92–3.38) reported by Tamirat et al., with an OR of 1.23 after inclusion of diagnostic facilities used as a conservative sensitivity analysis. After marginal transport to the current model, the primary-analysis values of P(T|A), P(T|D), P(T|H), and P(T|C) were 1.000, 0.827, 0.920, and 0.858, respectively; for C, the 2×2 intersection was re-solved using the primary marginal fC=197/658. None of these values constitutes a direct patient-level measurement of co-exposure in Gaza. The search for the residual effect of diagnostic delay identified no cancer-mortality study that explicitly controlled for T and allowed the mediated proportion to be estimated directly. Therefore, κD=0.5 was retained as the central structural assumption, with κD=0 and 1 used as the two extreme sensitivity analyses. Details are provided in **Supplementary Materials, Section 6**: **Part II**.

Historical Registry Trends, Back-Testing, and the Common Baseline

The numbers of registered cancer deaths in Gaza from 2016 through 2022 were 348, 474, 566, 548, 539, 777, and 915, respectively, and the corresponding crude registered mortality rates were 19.03, 25.26, 29.28, 27.54, 26.32, 36.88, and 42.24 per 100,000 population. The marked increase in the registered cancer mortality rate over 2016–2022 may reflect not only changes in underlying cancer mortality but also improvements in diagnosis, death registration, registry coverage, or reporting practices. Extrapolation of this historical trend may therefore partly extend changes in ascertainment rather than a purely biological increase in cancer mortality. The Poisson trend model with a population offset estimated β=0.1105, corresponding to an annual rate ratio for registered mortality of 1.117, and yielded a point prediction of 997.5 deaths for 2023 on the counterfactual registry scale. Pearson's chi-squared statistic was 41.20 with 5 residual degrees of freedom, giving a dispersion parameter of φ=8.24; the deviance-to-degrees-of-freedom ratio was 8.44, indicating marked overdispersion in the historical series. After correction using the Pearson dispersion parameter and 100,000 parameter draws, the common baseline was 997.2 (834.4–1189.3) deaths (**Table 3** below). The resulting estimate was higher than the companion study’s GBD-calibrated registry-equivalent estimate of approximately 906 deaths but was close to its Gaza-only extrapolations of 1,029 – 1,087 deaths based on 2019 – 2022 data. These estimates were not expected to coincide because they were derived using different source series, fitting periods, and reconstruction strategies; their difference therefore represents methodological variation rather than a numerical inconsistency between the two studies.

We also reviewed the Palestinian Ministry of Health Annual Health Report 2023 and its cancer-mortality annexes. Although the annexes included columns for the Gaza Strip, the Gaza entries were reported as unavailable (“/”), and no complete comparable full-year count of registered cancer deaths for Gaza in 2023 was provided. No complete observed full-year 2023 Gaza registry count was available for use as either the counterfactual baseline or a formal external-validation target[16].

Table 3. Historical inputs and fitted values for the Gaza cancer-mortality registry trend model

Year (t)	Mid-year population (P_t)	Registered cancer deaths (Y_t)	Crude registered mortality rate ($Y_t/P_t \times 100{,}000$)	Poisson-model fitted/extrapolated deaths ($\hat{\mu}_t$)
2016	1,828,614	348	19.03	378
2017	1,876,666	474	25.26	433.3
2018	1,932,843	566	29.28	498.4
2019	1,989,970	548	27.54	573
2020	2,047,969	539	26.32	658.6
2021	2,106,745	777	36.88	756.7
2022	2,166,269	915	42.24	869
2023	2,226,544	Not used as input	—	997.5

Note: The number of registered deaths in 2023 was not used to fit the model. The estimate of 997.5 deaths is the counterfactual point prediction on the registry scale under continuation of the 2016–2022 trend.

The absolute percentage errors from the five-fold expanding-window back-test ranged from 10.8% to 33.6%, with a MAPE of 20.5%, an MAE of 128.0 deaths, and an RMSE of 132.9 deaths. Complete fold-specific results are provided in **Supplementary Table S2**.

In the additional flat-rate sensitivity, the arithmetic mean of the exact 2019–2022 crude registered cancer mortality rates was 33.24 per 100,000. Applying this rate to the 2023 mid-year population yielded a point baseline of 740.2 deaths. After propagating between-year uncertainty in the mean rate, the median counterfactual baseline was 739.9 deaths (95% UI 573.8–906.6). Under this baseline, the primary six-factor model yielded 869.6 registered cancer deaths (95% UI 667.3–1082.2), an increment of 127.8 deaths (95% UI 65.5–215.0), and a relative increase of 17.44% (9.32%–27.70%).

Factor-Specific Analyses of the Six Additional Factors

The paired increment was 74.9 (14.8–158.1) deaths for diagnostic delay, 47.0 (3.6–102.4) deaths for psychosocial stress, and 38.9 (7.3–76.7) deaths in the exploratory particulate-matter analysis; none of the corresponding 95% UIs crossed 0. The estimates were 26.1 (−1.8–66.0) deaths for patient–provider communication barriers (Very poor+Poor), 6.3 (−3.1–18.0) deaths for health-care access barriers, and 2.3 (−10.4–15.9) deaths for health workforce loss or shortage; the intervals for these latter three factors included 0. For E, an exposure proxy was available only for October.

Table 4. Factor-specific analyses of the six factors on the counterfactual registry scale

Factor	Scenario deaths, median (95% UI)	Paired increment, median (95% UI)	Iterations with ΔD > 0 (%)	Increment UI crosses 0
A	1003.7 (839.4–1197.6)	6.3 (−3.1–18.0)	90	Yes
D	1073.8 (889.0–1298.5)	74.9 (14.8–158.1)	99.4	No
H	999.8 (835.8–1192.3)	2.3 (−10.4–15.9)	63.6	Yes
P	1045.6 (869.8–1253.7)	47.0 (3.6–102.4)	98.4	No
E, exploratory	1036.5 (864.8–1240.6)	38.9 (7.3–76.7)	99.3	No
C	1024.7 (854.4–1225.9)	26.1 (−1.8–66.0)	96.5	Yes

Note: The common baseline was 997.2 deaths (834.4–1189.3). All estimates are on the registry scale. The proportion of draws with ΔD>0 is neither a causal probability nor a posterior probability. The six rows are independent conditional scenarios and cannot be added together. E was prespecified as exploratory and was not included in the primary joint model.

Primary Six-Factor Joint Analysis and Exploratory Addition of Particulate Matter

Under the evidence-calibrated structure and the no-attenuation upper-bound assumption of g=1.00, the median wartime relative risk in the primary six-factor joint scenario was 1.698 (95% UI 1.373–2.108), and the annual multiplier after scaling to the three-month window was 1.1744 (1.0932–1.2770). The estimated number of registered deaths was 1172.8 (965.4–1424.6); in a paired comparison with the counterfactual baseline from the same simulation draw, the increment was 173.5 (90.9–286.5) deaths, corresponding to a relative increase of 17.44% (9.32%–27.70%). The paired difference from the treatment delay or interruption only reference was 121.6 (44.6–225.4) deaths. The T-only reference was used solely for model-reduction checks and comparison, and the paired difference cannot be obtained by directly subtracting the two marginal medians. When E was added using the exploratory October proxy of $\Delta x=4.1\ \mu g/m^3$, the extended seven-factor estimate increased to 1239.5 registered deaths (1013.6 – 1519.5), corresponding to an increment of 239.8 deaths (131.2 – 391.6) and a relative increase of 24.11% (13.48% – 37.94%).

In the illustrative registration-completeness analysis, applying 80% completeness converted the primary estimate of 1,172.8 registered deaths to 1,466.0 total deaths (95% UI 1,206.8 – 1,780.7). The corresponding paired total-death increment was 216.9 deaths (113.6 – 358.1). Across assumed completeness values of 70% – 85%, the implied total number of deaths ranged from 1,379.8 to 1,675.4. Under the flat 2019 – 2022 average-rate baseline, the corresponding estimate at 80% completeness was 1,087.0 total deaths (834.1 – 1,352.8). These values were deterministic scale conversions of the registered-death results rather than independent model estimates (**Supplementary Materials, Section 5: Table 9**).

In the Shapley decomposition of the primary six-factor model, diagnostic delay had the largest median allocation at 70.0 deaths (95% UI 14.1 – 146.2; 40.5%), followed by psychosocial stress at 59.1 deaths (4.5 – 129.4; 34.1%). The remaining factors each had median allocations of 19.4 deaths or fewer (**Supplementary Materials, Section 7: Supplementary Table S4B**). These values are model-based allocations rather than independently attributable deaths.

At κD=0, 0.5, and 1, the primary six-factor joint increments were 130.3 (67.0–214.5), 173.5 (90.9–286.5), and 224.7 (109.2–393.2) deaths, respectively, indicating that the residual pathway of diagnostic delay after treatment interruption remained an important source of structural uncertainty. Complete results are provided in **Supplementary Materials, Section 7: Supplementary Table S5A**.

Across the six overlap structures, median joint increments ranged from 171.4 to 184.9 deaths; the conservative Rao association for diagnostic delay and the Tamirat facility-adjusted association for communication produced estimates of 176.1 and 176.7 deaths, respectively. As λT decreased from 1 to 0, the joint increment decreased from 173.5 to 102.4 deaths. The within-combination additive excess-risk and full multiplicative bounds were 212.2 and 291.4 deaths, respectively. The 95% UIs for all fixed structural scenarios remained above 0. Compared with variation from the evidence-low to evidence-high overlap structures, κD, λT, and the combination rule produced larger changes. Complete numerical results are provided in **Supplementary Materials, Section 7: Supplementary Tables S5B–S5D**.

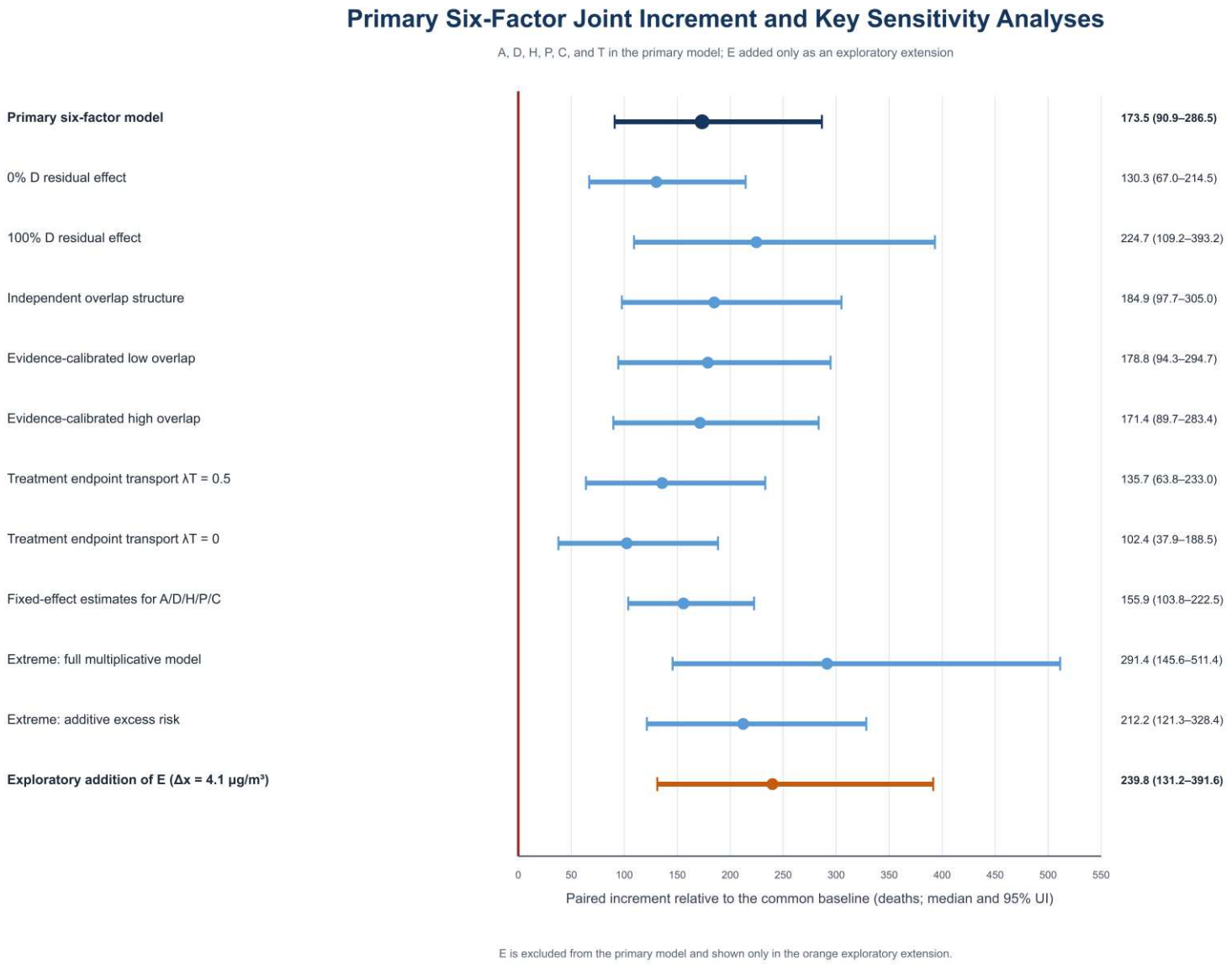


Figure 2. Increment in registered cancer deaths under the primary six-factor joint model and key sensitivity analyses.
Points indicate medians and horizontal lines indicate 95% uncertainty intervals from 100,000 Monte Carlo draws. The primary model combined health-care access barriers, diagnostic delay, health workforce loss or shortage, psychosocial stress, patient–provider communication barriers, and treatment delay or interruption. Particulate-matter exposure was excluded from the primary joint model and added only in the orange exploratory seven-factor extension using Δx=4.1 µg/m³. Full multiplication and additive excess risk are extreme structural explorations.

Factor-Specific, Mapping-Parameter, Baseline, and Program Sensitivity Analyses

In the factor-specific analyses, the effects of D and P remained positive under alternative f and g values and fixed-effect substitution. The fixed-effect increment for A was −2.8 (−5.1 to −0.6) deaths, opposite in direction to the random-effects primary analysis; the fixed-effect increment for E decreased to 1.3 (−0.3–3.0) deaths and varied markedly with Δx. H remained close to 0 across scenarios, and both the new and old definition scenarios for C retained wide UIs that crossed 0. Complete results are provided in **Supplementary Materials, Section 7: Supplementary Tables S6–S9**.

The f and g parameters primarily scaled the magnitude of the effects without changing their direction; the five baseline scenarios likewise did not change the overall pattern in which D, P, and E were positive, whereas the intervals for A, H, and C crossed 0. The choice of meta-analytic model had a greater effect on A and E, indicating that stable inferences for these factors should not be based solely on the point estimates from the primary model.

When the particulate-matter Δx was 0, the increment was 0 by definition. The satellite-based alternative scenario yielded −10.0 (−18.4 to −2.0) deaths, indicating only that the proxy concentration used was lower than that in the comparison period; the household-fuel smoke scenario yielded 97.5 (16.8–210.1) deaths. Both were factor-specific exploratory analyses of E and were not included in either the primary joint model or the exploratory joint extension. In the separately specified exploratory extension using the October proxy of Δx=4.1 µg/m³, inclusion of E increased the joint increment from 173.5 to 239.8 deaths. Detailed results are provided in **Supplementary Materials, Section 7: Supplementary Table S9A**.

In the primary six-factor joint model, the low, primary, and high values of all f parameters corresponded to increments of 112.6, 173.5, and 211.1 deaths, respectively. As g increased from 0.35 to 1.00, the corresponding increments increased from 60.7 to 173.5 deaths. Replacing the REML random-effects estimates for A, D, H, P, and C with fixed-effect estimates yielded an increment of 155.9 deaths. The three levels of the previous definition of C yielded increments ranging from 173.5 to 192.4 deaths. Across the five baseline scenarios, the joint increment ranged from 127.8 to 173.8 deaths; the flat 2019–2022 average-rate scenario produced the smallest increment, 127.8 deaths (95% UI 65.5–215.0), while preserving the relative increase of 17.44% (9.32%–27.70%). In the exploratory seven-factor extension, addition of E yielded increments of 173.5, 181.0, 239.8, and 297.2 deaths at Δx values of 0, 0.5, 4.1, and 7.2 μg/m³, respectively. The 95% UIs for all fixed scenarios remained above 0; detailed numerical results are provided in **Supplementary Materials, Section 7: Supplementary Table S10**.

All prespecified program-verification checks, including sampling validity, deterministic reproducibility, probability constraints, model-reduction identities, annual scaling, and Shapley additivity, were passed; complete results are provided in **Supplementary Materials, Section 7: Supplementary Table S3.**

Discussion

Main Findings

This study identified 263 standardized war-related factors from 1,341 valid records across 413 studies. The cancer-patient subset comprised 23 studies, 67 factor records, and 29 standardized factors; health services and systems accounted for 65.7% of the factor records. Based on cancer mortality registration and population trends in Gaza from 2016 through 2022, the projected baseline number of registered cancer deaths in 2023 was 997.2 (95% UI, 834.4–1189.3). Factor-specific analyses estimated death increments of 74.9 (14.8–158.1), 47.0 (3.6–102.4), and 38.9 (7.3–76.7) for diagnostic delay, psychosocial stress, and particulate-matter exposure, respectively; none of their 95% UIs crossed 0. The corresponding increments were 26.1 (−1.8–66.0) deaths for patient–provider communication barriers, 6.3 (−3.1–18.0) deaths for health-care access barriers, and 2.3 (−10.4–15.9) deaths for health workforce loss or shortage.

Under the no-attenuation upper-bound assumption of g=1.00, the primary six-factor model combining A, D, H, P, and C with treatment delay or interruption estimated 1172.8 registered cancer deaths (95% UI 965.4–1424.6), representing an increment of 173.5 deaths (90.9–286.5) relative to baseline, or a relative increase of 17.44% (9.32%–27.70%). Compared with the scenario considering treatment delay or interruption alone, the estimated increment increased by a further 121.6 deaths (44.6–225.4). Across g values of 0.35–1.00, the primary-model increment ranged from 60.7 to 173.5 deaths, so 173.5 represents the upper end of the prespecified realization scenarios rather than a single best estimate. Exploratory addition of particulate-matter exposure increased the increment to 239.8 deaths (131.2–391.6). Under different assumptions about the residual effect of diagnostic delay, the primary-model increment ranged from 130.3 to 224.7 deaths.

Placed in the context of other modelling studies from Gaza, our primary six-factor estimate of 173.5 additional registered cancer deaths (95% UI 90.9 – 286.5) for October – December 2023 was higher than the cancer-specific estimate reported by Abukmail et al., who projected 1,479 excess deaths across the non-communicable diseases included in their model between 7 October 2023 and 6 February 2024, of which 62 deaths (95% UI 20 – 117) were attributed to lung, colorectal, and breast cancer[2]. In our companion preprint, the separately reported point estimates were approximately 900 trajectory-based and 1,200 wartime registered cancer deaths for the whole of 2023, corresponding to a difference of approximately 300 deaths[4]. Our conservative flat-rate estimate of 127.8 deaths (95% UI 65.5 – 215.0) and primary estimate of 173.5 deaths therefore lay between the cancer-specific estimate of Abukmail et al. and the difference between the registry-scale point estimates in the companion preprint, while the exploratory estimate including particulate-matter exposure, 239.8 deaths (95% UI 131.2 – 391.6), was closer to the latter. These numerical comparisons should not be interpreted as direct validation or contradiction because Abukmail et al. included only three cancer sites and primarily modelled reduced treatment coverage, the companion preprint reconstructed annual cancer mortality, and the present study estimated a three-month conditional increment across all cancers under multiple interacting wartime factors. Moreover, the approximately 300-death comparison is a difference between separately reported point estimates rather than a paired excess-death estimate.

Comparison with the companion study becomes more consistent when the reporting scales are aligned. The present primary estimate of 1,172.8 registered deaths was close to the approximately 1,200 wartime registered deaths reported in the companion study. After illustrative conversion using 80% registration completeness, the implied total of 1,466.0 deaths was also close to the companion study’s modelled total wartime burden of approximately 1,400 deaths. It exceeded the crude GMS-derived approximation of approximately 1,200 total deaths by about 266 deaths; however, the flat-rate baseline produced a corresponding completeness-adjusted estimate of 1,087.0 deaths. The comparison therefore depended materially on the selected historical baseline and on whether results were expressed on the registered-death or total-death scale. The GMS-derived value was based on an approximate back-calculation and was not treated as a calibration target or gold-standard observation[4].

Strengths and Limitations

The main strength of this study is that it linked the identification of war-related factors, confirmation of the cancer-patient factor subset, effect-size evidence, and Gaza registry trends into a traceable analytical chain and examined the robustness of the results through sensitivity analyses of alternative baselines, effect models, exposure mappings, and joint structures. The study nevertheless has several limitations. First, the 2016–2022 registry series was short and could not distinguish changes in actual mortality from changes in diagnostic capacity and registration completeness; the extrapolated result therefore represents the counterfactual expectation under continuation of the prewar registration process rather than the actual total number of deaths in 2023. The rapid increase in registered mortality over 2016–2022 may therefore partly reflect improving diagnosis, ascertainment, and registry completeness. A flat-rate sensitivity based on the 2019–2022 average reduced the median counterfactual baseline from 997.2 to 739.9 deaths and the primary six-factor increment from 173.5 to 127.8 deaths, while leaving the relative increase unchanged. This indicates that the absolute death counts are sensitive to baseline specification, although the direction of the modelled association was preserved. The illustrative registration-completeness conversion introduced an additional structural assumption. Registration completeness was not directly measured for Gaza in 2023, and the conversion assumed that the same completeness applied to the counterfactual and wartime scenarios. Because registration may itself have deteriorated during the war, these converted values should be interpreted only as scale-reconciliation scenarios rather than as corrected estimates of the true total number of deaths. Second, the effect sizes were derived from different countries, cancer types, and health systems, creating unavoidable concerns about external applicability when transported to Gaza. Third, exposure proportions, time weights, and changes in particulate matter were represented only through

exploratory discrete scenarios, whereas the joint distribution and pathway-coverage rules could not be validated using patient-level data from Gaza. Fourth, the treatment factor used effects on overall survival or all-cause mortality, which were not fully aligned with the cancer-specific endpoints used for the additional factors. Accordingly, the results should be interpreted as conditional scenario estimates for assessing ranges of risk and policy scenarios, rather than as estimates of individual-level causal effects or definitive attribution of deaths to war. Moreover, the treatment delay or interruption parameter was derived from an SSRN preprint that had not completed peer review at the time of analysis; although its effect was transported under three λ_T scenarios, the joint estimate remains dependent on this external parameter. Ultimately, not all war-specific pathways were modelled, including destruction of oncology infrastructure, loss of specialised services, disrupted referral and supply chains, infection, malnutrition, and displacement. The omission of these pathways could bias the estimates downward. Conversely, the use of total wartime exposure proportions as proxies for incremental exposure, together with the no-attenuation assumption of g=1.00, could bias the estimates upward. The net direction of bias is therefore uncertain, and the primary estimate should be interpreted as a conditional upper-bound realization scenario under the specified assumptions rather than as a uniformly conservative estimate.

Continuity of Diagnosis and Treatment as a Core Pathway Linking War to Cancer Outcomes

Cancer care is highly sensitive to timing and continuity. Pathological diagnosis, imaging-based staging, referral, surgery, radiotherapy, and systemic therapy usually form a continuous care pathway, and disruption at any point may cause patients to miss an appropriate treatment window. The particular problem in conflict-affected settings is not simply a reduction in individual services, but simultaneous disruption to transport, referral, energy supplies, health-care personnel, medicine supplies, and hospital operations, resulting in systemic breaks in care processes that would otherwise be coordinated[1-3,6,20,22,32,72-74]. Early in the conflict, WHO had already reported fuel shortages, reduced hospital functionality, and difficulties for patients with cancer in accessing treatment; subsequent health-facility assessments also documented widespread effects on hospital services and referral capacity[75,76].

The positive pooled association for diagnostic delay in this study is consistent with the wider literature on the timeliness of cancer diagnosis. In a separately conducted all-cancer systematic review, Neal et al. concluded that expediting the diagnosis of symptomatic cancer was likely to improve stage at diagnosis, survival, and quality of life, while also emphasizing heterogeneity across cancer sites, delay definitions, and study methods[77]. Evidence concerning treatment delay is related but distinct: in a systematic review and meta-analysis of more than 1.27 million patients, Hanna et al. found that each four-week delay in cancer treatment was associated with increased mortality across several treatment indications[78]. Together, these evidence streams support treating diagnostic delay and treatment delay or interruption as related but separate parts of the cancer-care pathway. However, the studies included in our diagnostic-delay meta-analysis used different thresholds, cancer types, and clinical pathways. The pooled HR therefore compares the adverse delay state defined by each study with its reference group and cannot be interpreted as a fixed proportional increase in risk for each additional week of delay. Retaining the original definitions used by the studies avoided unsupported dose conversions, while also limiting interpretation of the findings in terms of a specific duration of delay.

Treatment delay or interruption served as a shared pathway in the joint model. Barriers related to health-care access, the health workforce, and communication may first reduce the probability that a patient receives timely treatment and subsequently affect survival through treatment interruption. Directly multiplying the full HRs for these factors by the HR for the treatment factor would risk counting the same treatment-continuity pathway more than once. This study reduced such duplication through pathway coverage and retention of partial independent effects, but these rules remain structural assumptions based on clinical reasoning and limited evidence about overlap. In particular, the treatment factor primarily used effects on overall survival or all-cause mortality, whereas the additional factors used cancer-specific mortality effects wherever possible. The λT sensitivity analysis showed that the joint increment remained positive but decreased markedly when the treatment-factor effect was reduced or removed, indicating that endpoint differences affected the magnitude of the result but could not fully account for the additional burden estimated by the model.

Interpretation of Health-System, Psychosocial, and Environmental Factors

Health-care access, the health workforce, and patient–provider communication jointly determine whether patients with cancer can actually enter and complete the care process, but the proxy measures used in previous studies do not fully correspond to a wartime environment. Insurance status, travel time, regional physician density, and social vulnerability generally reflect structural differences within health systems under ordinary conditions, whereas blockades, hospital closures, forced displacement, and disruption of referral routes represent more severe shocks to service delivery. Accordingly, the opposite directions of the random-effects and fixed-effect results for health-care access should not be interpreted as indicating that access barriers may be protective; rather, they show that differences in exposure definitions, study weights, and populations had substantial effects on the pooled estimate. Similarly, a pooled HR for the health workforce close to 1 does not indicate that workforce shortages are harmless. Effective cancer-care capacity in wartime depends on coordination among pathology, nursing, radiology, pharmacy, transport, and registry personnel, and physician density alone is unlikely to capture this team-based capacity.

The role of patient–provider communication should likewise not be reduced to whether the patient and provider speak the same language. Risk explanation, informed decision-making, health literacy, understanding of treatment plans, and patient navigation across institutions may all affect adherence and diagnostic delay[42,70,71,79]. This study used “Very poor+Poor” as the primary-analysis definition to distinguish clearly poor communication from communication experiences rated as average or acceptable; the previous definition, which included Fair in the barrier group, was retained as a sensitivity analysis to show how the classification boundary affected the result. Because the pooled interval crossed 1, this finding cannot establish that communication barriers independently increase cancer mortality, but it supports providing patient navigation, referral tracking, and clear risk communication as cancer services are restored.

Psychosocial stress may affect cancer outcomes through multiple pathways, including neuroendocrine function, inflammation, sleep, health behaviors, and treatment adherence. The positive pooled association in this study is compatible with evidence from populations that were not included in our meta-analysis. In a multi-cohort study of 13,349 UK Biobank participants living with and beyond cancer, with replication in 5,739 participants from the Finnish Public Sector study, psychological distress was associated with cancer mortality (pooled adjusted RR 1.57, 95% CI 1.37–1.79); adjustment for cancer stage attenuated but did not eliminate the association[80]. In Gaza, a survey of patients with breast cancer and studies of the general and displaced populations during the conflict documented substantial anxiety, depression, and persistent psychological distress.30,31,33 However, this evidence does not establish that three months of acute wartime stress would immediately produce the same cancer-specific mortality effect as longer-term psychological exposure. The psychosocial-stress result in this study should therefore be interpreted as a scenario indicating potential risk. Even if its short-term mortality effect remains uncertain, incorporating psychological screening, crisis intervention, caregiver support, and continuing contact into oncology services retains independent clinical value.

Meaning of the Joint Model and Public Health Implications

The value of the joint model lies not in producing an apparently precise total death count, but in incorporating overlap and shared pathways among factors into a common set of testable assumptions. The primary model neither directly multiplied the six factor-specific effect estimates nor summed the independently estimated death increments. Instead, it first constructed a joint distribution linking treatment delay or interruption with health-care access barriers, diagnostic delay, health workforce loss or shortage, psychosocial stress, and patient–provider communication barriers. It then applied pathway-coverage rules according to whether treatment was interrupted and calculated the expected effect across the 64 mutually exclusive exposure combinations. Particulate-matter exposure was excluded from this primary joint distribution because its Gaza exposure proxy was limited to one month, was derived from monitoring stations outside Gaza, and was inconsistent in direction with the satellite-based alternative. It was instead applied as a continuous area-level multiplier only in a separately labelled exploratory seven-factor extension. This approach reduced evident double counting, but did not resolve the fundamental absence of patient-level observations for the joint distribution. Variation in the results across association structures and settings for κD and λT is therefore part of the structural uncertainty in the primary joint estimate, while variation across particulate-matter concentration increments reflects uncertainty in the exploratory environmental extension.

From a public-health perspective, the findings support making the restoration of diagnostic capacity and the maintenance of treatment continuity central tasks in the emergency cancer response. Pathology, imaging, rapid referral, and linkage to treatment after diagnosis should be regarded as a complete service pathway rather than as separate programs. Workforce recovery should likewise extend beyond physician counts and ensure capacity in nursing, pathology, radiology, pharmacy, patient navigation, data registration, and medical transport. Psychosocial support should be embedded in oncology services, whereas environmental risks require ongoing monitoring and source differentiation. Diagnostic delay received the largest median Shapley allocation, reinforcing the importance of restoring pathology, imaging, rapid referral, and linkage to treatment alongside chemotherapy and other treatment services. However, Shapley values are mathematical allocations of the modelled increment under the specified joint distribution and pathway rules; they should not be interpreted as independently attributable deaths or used alone to rank resource priorities. In practical terms, the factor-specific increments and the primary six-factor joint-scenario estimate and the exploratory E-inclusive extension should be used to indicate the plausible order of magnitude of excess registered cancer deaths under a transparent set of assumptions, to compare alternative service-restoration and continuity-of-care strategies, to identify which structural assumptions most strongly influence the results, and to communicate uncertainty to planners and responders. They should not be used as observed death counts, as definitive estimates of deaths attributable to war, as individual-level causal effects, as precise forecasts of 2023 mortality, as a basis for legal or forensic attribution, or as the sole criterion for ranking factors or allocating resources. The factor-specific increments are conditional and non-additive; the joint estimate is a composite scenario that depends on exposure mapping, co-exposure, pathway coverage, endpoint transport, and unmodelled war-specific pathways. Omitted wartime pathways could bias the estimate downward, whereas upper-bound affected-burden mappings and the no-attenuation assumption of $g=1.00$ could bias it upward. The net direction of bias is therefore uncertain. These estimates are therefore intended to support assumption-explicit contingency planning and to generate hypotheses for validation with patient-level and registry data, not to provide a final accounting of war-related cancer mortality.

Conclusion

The systematic review identified 263 standardized factors from 1,341 factor records across 413 studies. On the basis of the disease and study-population fields and review of the original reports, it further identified a cancer-patient factor subset comprising 23 studies, 67 records, and 29 standardized factors. After effect-size studies were sought for each factor in the subset, no relevant studies were found for some factors, whereas all candidate studies for other factors were excluded after application of the eligibility criteria; usable effect estimates were ultimately available for six additional factors, all of which were evaluated in factor-specific models; five were included in the primary joint model, whereas particulate-matter exposure was retained as exploratory. Diagnostic delay and psychosocial stress showed relatively consistent positive signals; the particulate-matter result was sensitive to the effect model and concentration increment; and the uncertainty was greater for communication barriers, health-care access, and workforce shortages.

Against the common counterfactual registry baseline for 2023, the primary six-factor joint scenario produced an increment of 173.5 registered cancer deaths (95% UI 90.9–286.5) under the no-attenuation upper-bound assumption of $g=1.00$. Under the conservative flat 2019–2022 average-rate sensitivity, the corresponding increment was 127.8 deaths (95% UI 65.5–215.0). Across the prespecified realization assumptions of $g=0.35$–1.00, the corresponding primary-model increment ranged from 60.7 to 173.5 deaths; therefore, 173.5 deaths should be interpreted as an upper-bound scenario estimate rather than a single best estimate. Exploratory addition of particulate-matter exposure increased the estimate to 239.8 deaths (131.2–391.6). Treatment delay or interruption was used only as a joint factor and model reference, rather than as a new independent research result. The primary joint estimate depends on transporting conditional associations across populations, complete pathway coverage for A/H/C, retention of 50% of the log HR for D, an all-cause mortality proxy for treatment delay, and the assumed proportion of excess relative hazard realized within the three-month window. It should therefore be interpreted as a composite conditional scenario under structural assumptions.

References:

[1] Casolino, R. *et al.*, Integrating cancer into crisis: a global vision for action from WHO and partners. *The Lancet Oncology* **26**, e55 (2025).

[2] Abukmail, H. *et al.*, Modelling excess mortality from non-communicable diseases during wartime: application to the Gaza Strip, occupied Palestinian territories. *Popul. Health Metr.* **23**, 68 (2025).

[3] Gourd, E., Cancer care desperately impeded by fighting in Gaza. *The Lancet Oncology* **24**, e241 (2023).

[4] Luo, Z. *et al.*, in Estimating Cancer Mortality and Undiagnosed Cases Under Conflict: A Scenario-Based Reconstruction for Palestine, 2019-2023, (SSRN, 2025).

[5] Jawad, M. *et al.*, The impact of armed conflict on cancer among civilian populations in low- and middle-income countries: a systematic review. *Ecancermedicalscience* **14**, 1039 (2020).

[6] Halahleh, K. ,Gale, R. P., Cancer care in the Palestinian territories. *The Lancet Oncology* **19**, e359 (2018).

[7] Sphere, S., The Sphere Handbook. *(No Title)* (2018).

[8] Organization, W. H., in *Everybody's business: strengthening health systems to improve health outcomes: WHO's framework for action* (2007).

[9] Organization, W. H., Health resources and services availability monitoring system (HeRAMS): external evaluation report, July 2019. (2021).

[10] Organization, W. H., in Glossary of Health Emergency and Disaster Risk Management Terminology. Geneva: World Health Organization. 2020.

[11] UNDRR, F., Report of the open-ended intergovernmental expert working group on indicators and terminology relating to disaster risk reduction. *New York: United Nations* (2016).

[12] Des Combes, H. J., Hazard Information Profiles: UNDRR-ISC Hazard Information Profiles: An opportunity to better understand chemical hazards and associated risk management. *Chemistry International* **47**, 5 (2025).

[13] Solar, O. ,Irwin, A., A conceptual framework for action on the social determinants of health. (2010).

[14] Page, M. J. *et al.*, The PRISMA 2020 statement: an updated guideline for reporting systematic reviews. *BMJ (Clinical research ed.)* **372**, n71 (2021).

[15] Higgins, J. P. T. *et al.*, A tool to assess risk of bias in non-randomized follow-up studies of exposure effects (ROBINS-E). *Environ. Int.* **186**, 108602 (2024).

[16] Palestinian, M. O. H., Palestine Health Annual Report 2023, https://site.moh.ps/Content/Books/XgLftcbJzicWeKXt4WrZj23xsXqOurcWPKQlmzFSzUnv7p1jSEVmgG_pdx8duawOkhBVtXbW3YbLuJnKarGr1arROWT2UNKdlBrrMv7UQYvXT.pdf (2024).

[17] Palestinian, C. B. O. S., in Revised Population Estimates Based on the Final Results of the Population, Housing and Establishments Census, 2017, (Palestinian Central Bureau of Statistics
, Ramallah, 2023).

[18] United, N. O. F. T., Hostilities in the Gaza Strip and Israel | Flash Update #14, https://www.ochaopt.org/content/hostilities-gaza-strip-and-israel-flash-update-14 (2023).

[19] World, H. O., Health access: Barriers for patients in the occupied Palestinian territory — July 2023, https://www.emro.who.int/images/stories/July_2023_Monthly_2.pdf (2023).

[20] Bouquet, B. *et al.*, Comparative survival of cancer patients requiring Israeli permits to exit the Gaza Strip for health care: A retrospective cohort study from 2008 to 2017. *PLoS One* **16**, e251058 (2021).

[21] Ministry, O. H. P., Annual Health Report 2022: Southern Governorates – Gaza Strip, https://www.moh.gov.ps/portal/wp-content/uploads/2023/07/annual-english-202218-7-2023.pdf (2023).

[22] Palestinian, C. F. H. R., Women with Cancer Face Imminent Death in the Gaza Strip Amid Ongoing Genocide, https://pchrgaza.org/wp-content/uploads/2024/06/Cancer-patients-en-1.pdf (2024).

[23] Palestinian, C. F. H. R., The Silent Death: Cancer Patients Left to Die Waiting: Victims of Genocide in the Gaza Strip, https://pchrgaza.org/wp-content/uploads/2025/05/The-Silent-Death.pdf (2025).

[24] World, H. O., WHO teams deliver supplies to hospitals in Northern and Southern Gaza, https://www.who.int/news/item/27-12-2023-who-teams-deliver-supplies-to-hospitals-in-northern-and-southern-gaza (2023).

[25] United, N. O. F. T., Humanitarian Situation Update #265 | Gaza Strip, https://www.ochaopt.org/content/humanitarian-situation-update-265-gaza-strip (2025).

[26] Vamsi Gade, V. K. *et al.*, Real-World Data From India on Delays and Disruptions in Cervical Cancer Care Services During the COVID-19 Pandemic. *JCO Glob. Oncol.* **12**, e2500765 (2026).

[27] World, H. O., Health Impact of the Escalation of Violence, https://apps.who.int/gb/COVID-19/pdf_files/2023/13_11/Item1.pdf (2023).

[28] Peeperkorn, R. ,Casey, S., Opening remarks, UN Palais briefing, 21 December 2023, https://www.emro.who.int/media/news/opening-remarks-un-palais-briefing-21-december-2023.html (2023).

[29] Elhissi, J. H., Mapping Study for Cancer Care in the Gaza Strip, https://www.islamic-relief.ie/wp-content/uploads/2020/04/MappingCancerCareGaza.pdf (2022).

[30] Hejaz, H. A., Cross-sectional investigation of the effects of the war in Gaza on quality-of-life of breast cancer patients. *Eastern Mediterranean health journal = La revue de sante de la Mediterranee*
orientale = al-Majallah al-sihhiyah li-sharq al-mutawassit **31**, 101 (2025).

[31] Brugger, C. *et al.*, Changes in psychological distress during conflict escalation in an adult population-based cohort in the Gaza Strip: a longitudinal analysis. *EClinicalMedicine* **90**, (2025).

[32] Rihani, R. *et al.*, Restoring health and hope to displaced Gaza children with malignant disease at a cancer centre in Jordan. *Eastern Mediterranean health journal = La revue de sante de la Mediterranee*
orientale = al-Majallah al-sihhiyah li-sharq al-mutawassit **31**, 243 (2025).

[33] Albelbeisi, A. H. *et al.*, Prevalence and associated factors of mental health disorders among internally displaced persons in Gaza. *Eastern Mediterranean health journal = La revue de sante de la Mediterranee*
orientale = al-Majallah al-sihhiyah li-sharq al-mutawassit **31**, 81 (2025).

[34] Abu-Odah, H. *et al.*, Psychological distress and associated factors among Palestinian advanced cancer patients: A cross-sectional study. *Front. Psychol.* **Volume 13 - 2022**, (2022).

[35] Ashkelon, E. A., Air Monitoring Report, October 2022, https://www.e-a.org.il/prdFiles/%E2%80%8F%E2%80%8F%E2%80%8F%E2%80%8F%E2%80%8F%E2%80%8F%D7%93%D7%95%D7%97%20%D7%A0%D7%AA%D7%95%D7%A0%D7%99%20%D7%A0%D7%99%D7%98%D7%95%D7%A8%2010-2022.pdf (2022).

[36] Ashkelon, E. A., Air Monitoring Report, October 2023, https://www.e-a.org.il/prdFiles/%E2%80%8F%E2%80%8F%E2%80%8F%E2%80%8F%E2%80%8F%E2%80%8F%D7%93%D7%95%D7%97%20%D7%A0%D7%AA%D7%95%D7%A0%D7%99%20%D7%A0%D7%99%D7%98%D7%95%D7%A8%2010-2023.pdf (2023).

[37] IPC, F. R. C., Famine Review Committee: Gaza Strip, June 2024 – Conclusions and Recommendations, https://www.ipcinfo.org/fileadmin/user_upload/ipcinfo/docs/IPC_Famine_Review_Committee_Report_Gaza_June2024.pdf (2024).

[38] United, N. E. P., Environmental Impact of the Conflict in Gaza: Preliminary Assessment of Environmental Impacts, https://wedocs.unep.org/items/41dc66cb-c5be-4c59-8f28-c7ef9bc74fcd (2024).

[39] Mohamadi, B. *et al.*, Integrating InSAR coherence and air pollution detection satellites to study the impact of war on air quality. *Int. J. Appl. Earth Obs. Geoinf.* **142**, 104687 (2025).

[40] Asfour, B., Asia, M. R. ,Hejaz, H. A., Effects of October 2023 war on health care costs in Gaza. *Eastern Mediterranean health journal = La revue de sante de la Mediterranee orientale = al-Majallah al-sihhiyah li-sharq al-mutawassit* **31**, 254 (2025).

[41] Elsous, A. *et al.*, Unmet needs and health-related quality of life of breast cancer survivors: survey from Gaza Strip, Palestine. *Acta oncologica (Stockholm, Sweden)* **62**, 194 (2023).

[42] Tamirat, K. S. *et al.*, The effect of cultural and linguistic diversity on the timeliness of prostate cancer treatment: a registry-based retrospective cohort study. *Cancer causes & control : CCC* **36**, 1975 (2025).

[43] Stevens, G. A. *et al.*, Guidelines for Accurate and Transparent Health Estimates Reporting: the GATHER statement. *PLoS Med.* **13**, e1002056 (2016).

[44] Jiang, C. *et al.*, Transportation barriers, emergency room use, and mortality risk among US adults by cancer history. *JNCI: Journal of the National Cancer Institute* **115**, 815 (2023).

[45] Korn, S. M. *et al.*, Travel Time to Treating Facility and Mortality in Men With Prostate Cancer. *JAMA Netw. Open* **8**, e2546812 (2025).

[46] Smartt, A. A., Jang, E. S. ,Tyler, W. K., Is There an Association Between Insurance Status and Survival and Treatment of Primary Bone and Extremity Soft-tissue Sarcomas? A SEER Database Study. *Clinical Orthopaedics & Related Research* **478**, 527 (2019).

[47] Masoud, S. J. *et al.*, Social Vulnerability Index and Survivorship after Colorectal Cancer Resection. *J. Am. Coll. Surg.* **238**, 693 (2024).

[48] Zhao, Y. *et al.*, Influence of Diagnostic and Treatment Delays on Survival Outcomes in Patients With Locally Advanced Rectal Cancer: A Multi-Center Retrospective Cohort Study. *Cancer Med.* **15**, e71744 (2026).

[49] Hollenbeck, B. K. *et al.*, Delays in diagnosis and bladder cancer mortality. *Cancer.* **116**, 5235 (2010).

[50] Yin, L. X. *et al.*, Disease Profile and Oncologic Outcomes After Delayed Diagnosis of Human Papillomavirus – Associated Oropharyngeal Cancer. *Otolaryngology – Head and Neck Surgery* **165**, 830 (2021).

[51] Teppo, H. ,Alho, O., Comorbidity and diagnostic delay in cancer of the larynx, tongue and pharynx. *Oral Oncol.* **45**, 692 (2009).

[52] Fleming, N. H., Grade, M. M. ,Bendavid, E., Impact of primary care provider density on detection and diagnosis of cutaneous melanoma. *PLoS One* **13**, e200097 (2018).

[53] Blake, S. C. *et al.*, The association of dermatologist demographic density with melanoma survival in New South Wales, Australia. *Australas. J. Dermatol.* **64**, 425 (2023).

[54] Gadkaree, S. K. *et al.*, Role of physician density in predicting stage and survival for head and neck squamous cell carcinoma. *Head & Neck* **43**, 438 (2021).

[55] McDow, A. D. *et al.*, Impact of Endocrinologist and Surgeon Density on Well-Differentiated Thyroid Cancer Survival. *The American surgeon* **88**, 2626 (2022).

[56] Haas, J. S. *et al.*, Association of area sociodemographic characteristics and capacity for treatment with disparities in colorectal cancer care and mortality. *Cancer.* **117**, 4267 (2011).

[57] Freeman, V. L. *et al.*, Spatial access to primary care providers and colorectal cancer-specific survival in Cook County, Illinois. *Cancer Med.* **9**, 3211 (2020).

[58] Wan, N., Zhan, F. B., Lu, Y. ,Tiefenbacher, J. P., Access to healthcare and disparities in colorectal cancer survival in Texas. *Health Place* **18**, 321 (2012).

[59] Hamer, M., Chida, Y. ,Molloy, G. J., Psychological distress and cancer mortality. *J. Psychosom. Res.* **66**, 255 (2009).

[60] Jan, M. *et al.*, The roles of stress and social support in prostate cancer mortality. *Scand. J. Urol.* **50**, 47 (2016).

[61] Lu, D. *et al.*, Psychologic Distress Is Associated with Cancer-Specific Mortality among Patients with Cervical Cancer. *Cancer Res.* **79**, 3965 (2019).

[62] Wang, F. *et al.*, Social Support, Social Strain, Stressful Life Events and Mortality Among Postmenopausal Women With Breast Cancer. *Psycho-Oncol.* **33**, e70013 (2024).

[63] Poole, E. M. *et al.*, A prospective study of phobic anxiety, risk of ovarian cancer, and survival among patients. *Cancer. Causes. Control.* **27**, 661 (2016).

[64] Coleman, C. J. *et al.*, Greenness, air pollution, and mortality risk: A U.S. cohort study of cancer patients and survivors. *Environ. Int.* **157**, 106797 (2021).

[65] Liu, C. *et al.*, The association between ambient PM2.5's constituents exposure and cervical cancer survival. *Environ. Res.* **263**, 119928 (2024).

[66] Cheng, I. *et al.*, Outdoor ambient air pollution and breast cancer survival among California participants of the Multiethnic Cohort Study. *Environ. Int.* **161**, 107088 (2022).

[67] Hu, P. *et al.*, Long-term exposure to fine particulate matter constituents and the prognosis of oral cancer patients: A prospective study in Southeastern China. *J. Hazard. Mater.* **487**, 137304 (2025).

[68] Ou, J. Y. *et al.*, Fine Particulate Matter Air Pollution and Mortality among Pediatric, Adolescent, and Young Adult Cancer Patients. *Cancer Epidemiology, Biomarkers & Prevention* **29**, 1929 (2020).

[69] Su, M. *et al.*, The association between exposure to PM2.5 components from coal combustion and mortality in female breast cancer patients. *Environ. Res. Lett.* **18**, 104001 (2023).

[70] Spiegel, D. Y. *et al.*, Non – English Language Preference and Breast Cancer Outcomes. *JAMA Netw. Open* **8**, e2514036 (2025).

[71] Yelorda, K. L. *et al.*, Association of Cumulative Social Risk and Cancer-Specific Survival Among Patients With Advanced Colorectal Cancer. *Dis. Colon. Rectum.* **68**, 1085 (2025).

[72] World, H. O., WHO Press Conference: Update on health situation in Gaza - 21 December 2023, https://www.unognewsroom.org/teleprompter/en/1992/who-press-conference-update-on-health-situation-in-gaza-21-december-2023/5901 (2023).

[73] World, H. O., WHO Director-General's opening remarks at the Member State information session on Health Emergencies – 13 November 2023 - occupied Palestinian territory, https://reliefweb.int/report/occupied-palestinian-territory/who-director-generals-opening-remarks-member-state-information-session-health-emergencies-13-november-2023 (2023).

[74] Massad, S. *et al.*, Challenges of access to care for children with cancer living in the Gaza Strip/occupied Palestinian territory in 2022: a cross-sectional study. *BMJ Glob. Health* **11**, (2026).

[75] World, H. O. R. O., As Gaza ' s health system disintegrates, WHO calls for safe passage of fuel, supplies for health facilities, https://www.emro.who.int/opt/news/as-gazas-health-system-disintegrates-who-calls-for-safe-passage-of-fuel-supplies-for-health-facilities.html (2023).

[76] World, H. O., HeRAMS occupied Palestinian territory: Gaza snapshot September 2024 - all hospitals, https://www.who.int/publications/m/item/herams-opt-gaza-snapshot-2024-09-hospitals-en (2024).

[77] Neal, R. D. *et al.*, Is increased time to diagnosis and treatment in symptomatic cancer associated with poorer outcomes? Systematic review. *Br. J. Cancer* **112**, S92 (2015).

[78] Hanna, T. P. *et al.*, Mortality due to cancer treatment delay: systematic review and meta-analysis. *BMJ (Clinical research ed.)* **371**, m4087 (2020).

[79] Han, J. *et al.*, Primary language and its association with patient-reported treatment adherence and satisfaction in genitourinary oncology. *Cancer Treatment and Research Communications* **49**, 101452 (2026).

[80] Miller, N. E. *et al.*, Mediators of the association between psychological distress and mortality in people diagnosed with cancer. *Nat. Commun.* **16**, 11216 (2025).

Supplementary Files

This is a list of supplementary files associated with this preprint. Click to download.

- ExcelTable1.xlsx
- ExcelTable2.xlsx
- ExcelTable3.xlsx
- ExcelTable4.xlsx
- SupplementaryMaterials.docx